Screening of Small Molecule Regulators of Autophagy and Establishment of Mode of Action Analysis Method of Anti-cancer Drugs

January 2018

Osamu SANO

Screening of Small Molecule Regulators of Autophagy and Establishment of Mode of Action Analysis Method of Anti-cancer Drugs

A Dissertation Submitted to
the Graduate School of Life and Environmental Sciences,
the University of Tsukuba
in Partial Fulfillment of the Requirements
for the Degree of Doctor of Philosophy in Biological Science
(Doctoral Program in Biological Sciences)

Osamu SANO

Table of Contents

Abstract

Elucidation of biological phenomena by small molecules has been widely performed from long ago. Furthermore, in recent years, with the development of science and technology, chemical screening using more than 1,000 compounds has been widely conducted to identify novel biology and therapeutic drug candidate in industries and academia. The purpose of this study is to identify hit compounds that regulate biological phenomena and their target molecules through chemical screening and to analyze the mechanism of action of hit compounds.

In the first chapter, I focused on autophagy which is reported to be associated with various diseases especially in central nervous system and cancer, and have performed high content screening to identify autophagy regulators. I identified a hit compound named vacuolin-1, which is a target unknown compound. In order to identify the molecular target of vacuolin-1, I developed an algorithm to quantify cell morphology from images obtained at screening and clarified that vacuolin-1 inhibits PIKfyve by classifying hit compounds. More detailed analysis revealed that vacuolin-1 inhibits autophagy by suppressing vesicular transport from *Golgi* to endosome and lysosomal maturation.

In the second chapter, I clarified the mechanism of action of serine palmitoyl transferase (SPT) inhibitors that I had found as an attractive target to regulate cancer metabolism. In order to elucidate the mechanism of action, I constructed new chemical library containing about 3,000 biologically annotated compounds. In screening of compounds which affect cancer cell growth inhibitory activity of SPT inhibitors, I identified 32 compounds which attenuated cell growth inhibition induced by SPT inhibitors. Pathway enrichment analysis using these hit compounds revealed that prostaglandin production pathway is highly related with SPT inhibitor-induced cancer cell growth inhibition. More detail analysis showed that SPT inhibitor promotes cell death by activating prostaglandin production pathway through induction of expression

of COX-2.

In conclusion, I have successfully identified hit compounds that regulate biological phenomena and their target molecules through chemical screening and have analyzed the mechanism of action of hit compounds. It will be possible that my chemical screening methods for autophagy regulating compounds and for mechanism of action (MOA) analysis of anti-cancer drugs are widely applicable to identify autophagy inducer and to analyze MOA of other anti-cancer drugs.

Abbreviations

COX-2	Cycloxygenase-2
FBS	fetal bovine serum
HCS	high-content screening
LDH	lactate dehydrogenase
MOA	mechanisms of action
M6PR	mannose 6-phosphate receptor
SPT	Serine palmitoyl transferase
vATPase	vacuolar ATPase

General Introduction

Elucidation of biological phenomena is supported by the development of various analytical techniques and methodologies. Imaging of physiological state of biomolecules and cells using fluorescent probes and cell assays using compounds that specifically inhibit the function of certain biomolecules have also been utilized for a long time [1-4]. Particularly in recent years, the dramatic improvement of automated imaging devices and robotics technology allowed us to perform chemical screening at ultra-high throughput [5-8]. As a result, it has become possible to identify hit compounds with a shorter period of time and with higher probability than before. This achievement has made a great contribution not only to the advancement of life science, but also to the identification of medicines and new physiologically functional substances, so that the importance of chemical screening using cells is recognized not only by pharmaceutical companies but also by academia [9-13].

Successful chemical screening requires sophisticated primary phenotypic screening assay systems for identifying hit compounds, target proteins of the hit compounds, and precise compound profiling for revealing the mechanisms of action (MOA). Recently image-based high-content screening (HCS) using automated imaging devises has been recognized as a powerful methodology for identifying new chemical tools [14, 15]. HCS enables us to simultaneously measure multiple features of cellular phenotypes and obtain phenotypic profiling data; therefore, profiling using parameters obtained from cellular morphological property provides indispensable information about hit compounds.

Target identification of hit compounds remains challenging. To date, target identification methods that use chemical proteomics have been developed, and they have uncovered many unique target proteins associated with bioactive compounds [16-19]. To determine the target molecules of compounds without affinity tags, small-molecular profiling based on biological descriptor and cell morphology has been

developed [20, 21]. A method called cell painting utilizes fluorescent dyes to stain specific cellular components and clusters compounds based on morphological profiles [22]. By combining the above methods, although the probability of target identification has increased [23, 24], the establishment thereof is still not high. Therefore, it is important to build a new target identification platform.

It is also a critical step to understand the MOA for hit compounds. There are two commonly accepted methods for analyzing the MOA of hit compounds. One method involves a target-specific hypothesis-based approach that combines known information with newly obtained data from transcriptome and metabolome analyses [25]. The other method involves a discovery-based approach involving a functional genomics analysis of whole genome siRNA or shRNA [26]. Functional genomics analyses have provided many novel possibilities with regard to target relationships and thus represent a powerful approach for the identification of relatively novel targets. However, these unbiased siRNA- or shRNA-based approaches share the fundamental challenges of off-target effect, knockdown efficiency, protein turnover, and compensatory reactions [27, 28]. The establishment of alternative methods would be valuable to our understanding of the MOA of hit compounds.

In this study, I tried to establish highly informative chemical screening platform to identify hit compounds and their target molecules, and furthermore to analyze how hit compounds induce the desired phenotype. In the first chapter, I performed chemical screening to identify autophagy regulators. Autophagy is an intracellular catabolic reaction induced when unnecessary proteins accumulate in cells due to aging or stress, and is reported to be closely related to various diseases such as Alzheimer disease and cancer [29]. However, it largely remains unclear about the detailed mechanism of regulating autophagy. Because autophagy regulator is expected to be a novel therapeutic candidate, I developed a high content screening system to visualize and

quantify autophagy in multiple stages and performed chemical screening. I also tried target identification and MOA analysis of hit compounds by using cellular morphological information obtained at primary screening.

In the second chapter, I also worked on applying compound screening methods to elucidate the MOA of anti-cancer drugs. Today, identification of patient stratification marker allows leading higher success rate for drug development, and importance of elucidating the mechanism of action of anti-cancer drugs is increasing year by year [30, 31]. To elucidate the MOA of anticancer drugs, unbiased approach such as transcriptome or metabolome analysis, cancer cell panel assay, or genome wide siRNA screening are widely used. However, it is a problem that much labor and a large cost are required in either method. Therefore, by establishing a library of compounds with known MOA and constructing a screening system platform for combination with anti-cancer drugs, I tried to elucidate the mechanism of action of SPT inhibitors which I identified as a novel anti-cancer drug candidate.

Part I

Vacuolin-1 inhibits autophagy by impairing lysosomal maturation via PIKfyve inhibition

Abstract

Lysosomal protein degradation via autophagy strictly regulates cellular protein homeostasis. Herein I performed high-content screening to identify compounds that inhibit autophagy pathways. I obtained 11 hit compounds and performed cluster analysis using cellular morphological information. As a result, Vacuolin-1, which induces the formation of giant vacuoles and is a target unknown compound, was clustered with the known PIKfyve inhibitor YM201636. I further demonstrated that vacuolin-1 is a potent PIKfyve inhibitor, and I finally concluded that PIKfyve inhibitors are novel chemical tool for regulating autophagy.

Introduction

Sweeney et al. have analyzed the discovery strategies and the molecular mechanism of action (MMOA) for new molecular entities and new biologics that were approved by the US Food and Drug Administration between 1999 and 2008 to investigate whether some strategies have been more successful than others in the discovery of new drugs [32]. The results showed that the contribution of phenotypic screening to the discovery of first-in-class small-molecule drugs exceeded that of target-based approaches. Therefore, in both pharmaceutical and academic fields, phenotypic drug discovery has been recognized again as an essential process for discovering chemical tools that can unveil new therapeutic targets and new disease mechanism by previously undescribed mechanisms of action [10, 32]. Successful phenotypic screening requires sophisticated primary phenotypic screening assay systems for identifying hit compounds and precise compound profiling for revealing the mechanisms of action and target proteins of the hit compounds. High-content screening (HCS) has been recognized as a powerful methodology for identifying new chemical tools [33]. HCS enables us to simultaneously measure multiple features of cellular phenotypes and obtain phenotypic profiling data; therefore, profiling using parameters obtained from cellular morphological property provides indispensable information about hit compounds [34, 35].

Target identification of hit compounds obtained via phenotypic screening remains challenging, and this process has been considered a major bottleneck of phenotypic screening. To date, target identification methods that use chemical proteomics have been developed, and they have uncovered many unique target proteins associated with bioactive compounds [36, 37]. Although these are useful methods, they require mass spectrometry instrumentation and further chemical syntheses to add tags to compounds of interest without deteriorating their activities. To determine the target molecules of compounds without affinity tags, a profiling analysis of small-molecules based on biological descriptor and cell morphology has been developed. A method called cell painting utilizes fluorescent dyes to stain specific cellular components for clustering compounds based on morphological profiles [38, 39]. CellProfiler and Morphobase have also been developed to obtain multidimensional parameters obtained from image-based analysis [40, 41].

Macroautophagy (hereafter referred to as autophagy) is a catabolic process that results in the lysosomal degradation of bulk cytoplasmic contents [42-44]. Serum deprivation or unnecessary protein accumulation triggers autophagy to promote autophagosome formation and subsequent fusion to the lysosome, resulting in clearance of the unnecessary protein. The molecular bases of autophagy have been studied mainly

in yeast, and responsible genes have been identified using autophagy-defective mutants. In particular, a series of proteins called Atg (autophagy-related) have been identified to function as key drivers that modulate autophagy, and presently, more than 30 genes encoding Atg proteins have been discovered in yeast [45]. One Atg protein, Atg8, is a ubiquitin-like protein required for autophagosome formation. After being conjugated to the lipid phosphatidylethanolamine by a ubiquitin-like system, Atg8 is involved in the tethering and hemifusion of membranes [46]. The mechanism of autophagy was conserved during evolution among species ranging from yeast to mammals. When autophagy is activated, unlipidated LC3 (referred as LC3-I), the mammalian homologue of Atg8, was lipidated by addition of phosphatidylethanolamine, and lipidated LC3 (referred as LC3-II) is anchored to autophagosomes until it is degraded in the lysosome; therefore, it is widely used to monitor autophagy [47]. However, LC3 accumulation could occur in not only autophagy induction but also decline of autophagy flux in the late-stage. It is difficult to distinguish autophagy induction from inhibition by only monitoring LC3 accumulation.

Lysosome maturation is an important process for autophagy because fusion between the autophagosome and lysosome is the final step of autophagy. Lysosomes are highly acidified compartments (pH 4.5–5.0), and this pH gradient is generated and maintained

by a vacuolar membrane proton pump named vacuolar ATPase (vATPase). Lysosomes contain a large number of proteases and hydrolases and degrade unnecessary cellular proteins and organelles. These lysosomal enzymes are synthesized on the endoplasmic reticulum and transported to Golgi bodies before their subsequent delivery to transport vesicles via a mannose 6-phosphate receptor (M6PR)-dependent pathway and are finally delivered to lysosomes via small GTPase family protein-dependent pathway [48, 49]. Rab7 is localized to the late endosome, and it functions as a key regulator of vesicular transport to lysosomes and late endosomes [50]. Rab7 has also been reported to regulate fusion between the autophagosome and lysosome [51].

Although the molecular mechanism of autophagy has been intensely studied, there are few chemical tools regulating autophagy whose target has not been unidentified. Bafilomycin A1 is a well-known inhibitor of autophagy which inhibits vATPase and suppresses fusion of autophagosomes with lysosomes besides the acidification of endosomes and transport of lysosomal proteases to lysosomes [52]. However, the other target molecules involved in autophagy inhibition largely remain unclear. In this study, we used HCS to identify inhibitors of autophagy and performed target identification of hit compounds by cluster analysis using morphological information.

Materials and Methods

Materials

E64d and pepstatin A were purchased from Peptide Institute Inc. Other reagents were obtained from Life technologies unless otherwise specified.

Plasmid constructions

The plasmid encoding LC3 was purchased from Ultimate ORF collection. Open reading frame of LC3 was amplified by PCR and the PCR product was digested and insert into pAcGFP-C1 (Clontech Laboratories) and further inserted to pmCherry-C1 (Clontech Laboratories) to construct mCherry-AcGFP LC3 plasmid. DNA fragment containing mCherry-AcGFP LC3 was inserted in pEntr11 vector, and promoter region of pTRE-Tight (Clontech Laboratories) was inserted in pEnt5' vectors. pEnt5'-pTight promoter and pEntr11-mCherry-AcGFP-LC3 were integrated into pLenti6.4 vector by using multisite Gateway reaction kit (Thermofisher). For tet repressor expression, the sequence from TR to blasticidin of pLenti6/TR (Thermofisher) was replaced to rtTA-IRES-Neo sequence.

Antibodies

Anti-rab7 (9367S; used at 1/100 dilution for immuno-cytochemistry) and anti-beta-actin (4970S; used at 1/1000 dilution for western blotting) were purchased from Cell Signalling Technologies. Anti-M6PR (AB2733; used at 1/1000 dilution for immuno-cytochemistry) and anti-LAMP2 (AB25631; used at 1/250 dilution for immuno-cytochemistry) were purchased from Abcam. Anti-p62 (PM045; used at 1/2000 dilution for immuno-cytochemistry) and anti-LC3 (PM036; used at 1/1000 dilution for immuno-cytochemistry, and 1/2000 dilution for western blotting) were purchased from MBL.

Compounds

Tocriscreen (Tocris Bioscience) and StemSelect Small Molecule Regulators (Merck Millipore) were dissolved in DMSO (10 mM). Biologically annotated compounds were also collected to create a screening compound library. Bafilomycin A1, vacuolin-1, and YM201636 were purchased from Millipore, Tocris, and Selleck, respectively.

Cell line

HeLa cells were purchased from American Type Culture Collection (ATCC) and maintained in EME medium (EMEM) supplemented with 10% fetal bovine serum (FBS)

and non-essential amino acids. H4 cells were purchased from ATCC and maintained in DME medium (DMEM) supplemented with 10% FBS. For establishment of H4 cells with doxycycline-inducible mCherry-AcGFP LC3, mCherry-AcGFP LC3 and rtTA-IRES-neo viruses were transduced to H4 cells following the manufacturer's protocol, and stable cell line was cloned by dual-selection with neomycin and blasticidin and subsequent serial dilution.

HCS for LC3

HeLa cells were seeded in black clear-bottom 384-well imaging plates (Corning #3985) and treated with compounds for 6 or 24 h. Cells were fixed with 4% paraformaldehyde (Wako Pure Chemicals) and permeabilized with 50 μg/mL of digitonin (Wako) in PBS containing 0.1% gelatin (Wako). After washing with PBS containing 0.1% gelatin, cells were incubated with anti-LC3 antibody for 1 h, followed by incubation with anti-rabbit antibody conjugated with Alexa Fluor-488 and Hoechst 33258 for 1 h. After washing with PBS containing 0.1% gelatin, PBS was added to cells, which were stored at 4°C until measurement. Cell images were captured by the IN Cell Analyzer 6000 (GE Healthcare Japan) using ×20 or ×40 objective lens. LC3 staining intensity was calculated from captured images using the IN Cell Developer Toolbox (GE Healthcare

Japan).

HCS for proteins other than LC3

HeLa cells were seeded in black clear-bottom 384-well imaging plates and treated with compounds for 24 h. Cells were fixed with 4% paraformaldehyde and permeabilized with 0.1% Triton X-100 (Wako) in 10% goat sera for 1 h. After washing with PBS containing 0.1% Triton X-100, cells were incubated with antibodies for 24 h at 4°C, followed by incubation with secondary antibodies conjugated with Alexa Fluor-488 or Alexa Fluor-647 and Hoechst 33258 for 1 h at room temperature. After washing with PBS containing 0.1% Triton X-100, PBS was added to cells, which were stored at 4°C until measurement. Cell images were captured using the IN Cell Analyzer 6000. As shown in Table 2, several parameters were calculated from the captured images using the IN Cell Developer Toolbox by referring to the reference [40]. Image processing includes the following four steps;

Step 1: “Nuclei” segmentation using images of Hoechst staining. "Nuclear center" was predefined as a seed region of nuclear using objective segmentation module and postprocessing nodes, such as erosion and sieve. "Nuclei" was defined as the nuclear region that corresponded to "nuclear center" by the objective segmentation module.

Postprocessing nodes, such as clump breaking using "Nuclear center", erosion, sieve, and border object removal were used to separate close nuclei and properly segment the diverse nuclear phenotypes.

Step 2: “Cell” segmentation using images of Hoechst staining. “Cell” was defined as the cellular regions by the objective segmentation module with high sensitivity to detect weak signal. Postprocessing nodes such as erosion, clump breaking using "Nuclei", sieve, and fill holes were used to separate close cells properly.

Step 3: "Granule" segmentation. The immunofluorescence images of LC3, p62, LAMP2, and rab7 were used to detect textures, such as granules and vesicles, which were recognized by the vesicle segmentation module. "Cell" was linked with "Granule" using one to many target linking to quantify the area or density x area of Granule in each cells.

Step 4: Measure nodes. After individual cells were segmented, 17 user-defined descriptors (Table 2) were calculated for each cell.

Western blotting

Cells were collected and lysed in PBS containing 2% Triton X-100 and a protease inhibitor cocktail (Roche). The lysate was boiled with an SDS sample buffer (Bio-Rad)

containing 100 μM DTT. Samples were electrophoresed on a 5–20% of SDS polyacrylamide gel (ATTO), transferred to a PVDF membrane using an iBLOT apparatus, and immunodetected with the antibodies as mentioned above.

Tandem LC3 assay

H4 cells stably expressing tet-inducible mCherry-GFP-LC3 were seeded in F150 flasks in the presence of 1 μg/mL of doxycycline for 48 h. Cells were re-seeded in black clear-bottom 384-well plates and were treated with each compound for 24 h and fixed with 4% paraformaldehyde. Nuclei were stained with Hoechst 33342. Images were captured using the IN Cell Analyzer 6000.

siRNA transfection

HeLa cells were transfected with a final concentration of 30 nM siRNA. RNAiMAX was used for the reverse transfection according to the manufacturer's instructions (Life Technologies). To silence PIKfyve, specific siRNAs (Silencer® Select Pre-designed siRNA from Life Technologies; s47254, s47255, and s27256) targeting PIKfyve were used. Forty-eight hours after siRNA transfection, cells were harvested for real-time RT-PCR analysis using 1-step cells to CT reagent, and the knockdown of PIKfyve mRNA was

confirmed using TaqMan probes (Hs00381995_m1). Seventy-two hours after siRNA transfection, cell morphology was observed.

Kinase assay against PIKfyve

Vacuolin-1 and YM201636 were profiled using the commercially available Kd ELECT screening service (DiscoveRx) as previously described [53, 54]. Briefly, Kinase-tagged T7 phage strains were prepared in an *E. coli* host derived from the BL21 strain. Streptavidin-coated magnetic beads were treated with biotinylated small molecule ligands for 30 minutes at room temperature to generate affinity resins for kinase assays. Binding reactions were prepared by mixing kinases, affinity beads with ligands, and test compounds in 1×binding buffer (20% SeaBlock (Merck Millipore), 0.17× PBS, 0.05% Tween 20, 6 mM DTT). The beads washed with wash buffer (1× PBS, 0.05% Tween 20) and then re-suspended in elution buffer (1× PBS, 0.05% Tween 20, 0.5 μM non-biotinylated affinity ligand) and incubated at room temperature with shaking for 30 minutes. The kinase concentration in the eluates was measured by qPCR (Fig. 6). More detailed information is described in the DixcoveRX homepage; https://www.discoverx.com/technologies-platforms/competitive-binding-technology/kinomescan-technology-platform

Cluster analysis of hit compounds

All calculated data were normalized in each assay using the Z-scoring method and then analysed by hierarchical cluster analysis (Ward's method) with TIBCO Spotfire software (TIBCO).

Pearson's correlation coefficient

Pearson's correlation coefficient (Rp) was calculated using the following equation:

$$\mathrm{Rp} = \frac{\sum_{i=1}^{N}(x_i - \bar{x})(y_i - \bar{y})}{\sqrt{\sum_{i=1}^{N}(x_i - \bar{x})^2}\sqrt{\sum_{i=1}^{N}(y_i - \bar{y})^2}},$$

where N equals the 17 assay results and x_i and y_i are the activity values in each assay for compounds A and B, respectively.

Results and Discussion

Establishment of an HCS assay for autophagy regulators

The goals of this study were to obtain blockers of lysosomal protein degradation. I first analysed the morphological changes of cells treated with Bafilomycin A1 (Fig. 1) to define the criteria for hit compounds. I examined immunestained pattern of LC3 as an autophagy-related marker. I captured cell images using the IN Cell Analyzer 6000 high-content imager and quantified the fluorescent intensity using the IN Cell Developer Toolbox. As shown in Fig. 2A and 2B, bafilomycin A1 treatment for 6 h induced LC3 dot formation, and LC3 dot formation was further increased following treatment for 24 h. I also immunostained cells with anti-p62 antibodies. p62 is a multifunctional protein that plays a crucial role in autophagy by linking autophagy with the proteasome pathway [55, 56]. Together with LC3 accumulation, p62 was significantly accumulated in bafilomycin A1-treated cells, indicating that cellular autophagy flux was inhibited. Moreover, immunostainings of rab7 as a late endosome marker and LAMP2 as a lysosome marker showed significant accumulation of rab7-positive vesicles and LAMP2-positive lysosomes in bafilomycin A1-treated cells (Fig. 2A, and 2B). Therefore, I defined simultaneous accumulation of LC3, p62, rab7, and LAMP2 as features of lysosomal dysfunction phenotype including that was seen in

bafilomycin A1-treated cells.

Identification of autophagy inhibitors: Cluster analysis revealed that five inhibitors regulate autophagy and endosomal trafficking

I performed primary screening of approximately 1,500 known bioactive compounds at a concentration of 3 μM to identify blockers of autophagy and endocytic pathways. I monitored LC3 dot formation after 6 and 24 h of treatment with the test compounds. Regarding p62, rab7, and LAMP2 accumulation following 24 h of treatment with the test compounds, I scored each sample based on the intensity of immunofluorescence, and the hit criterion was an immunofluorescence intensity at least three standard deviations greater than the mean intensity of immunofluorescence in DMSO-treated samples. As a consequence, 11 compounds as primary hit compounds were selected (Table 1). Because hit compounds from phenotypic screening have generally several modes of action, the establishment of classification methods of hit compounds improves the subsequent target identification steps. To classify the hit compounds, I utilized primary screening data, and captured images were re-analysed using a custom-made analysis algorism. In total, 17 parameters reflecting morphological changes were calculated as shown in Fig. 3A and Table 2. I put the utmost importance on

experimental reproducibility and robustness of the parameters to avoid variability from plate to plate or batch to batch, although, theoretically, I could calculate more parameters. In addition, except for the parameters used in the primary screening (the intensity of LC3, p62, rab7, LAMP2), I calculated morphological parameters mainly from images of Hoechst 33258 staining (10 out of 17 parameters) to apply this approach for other high content screening. Finally, I selected 17 parameters. All obtained data were analysed via hierarchical clustering of the activities using Ward's method in TIBCO Spotfire software. As a result of the hierarchical cluster analysis, compounds that produced similar morphological changes were classified into the same cluster, enabling me to visually determine that they have similar molecular targets and signalling pathways. Via cluster analysis, 11 hit compounds were classified into five biological clusters (Fig. 3B). I found that three well-known tubulin disruptors (vincristine, vinblastine, and colchicine), one tubulin stabilizer (Taxol), and KF 38789, which was originally identified as a selective inhibitor of P-selectin-mediated cell adhesion [57] and recently identified as a tubulin disruptor [58], were classified into the same cluster. This result suggested that the calculated parameters and cluster analysis work well and reflect the features of cellular status. Interestingly, bafilomycin A1, which was used as the positive control, did not cluster with any other compound, and

this result suggested that other hit compounds have different modes of action regarding their inhibitory effects on the autophagy pathway. Two actin disruptors and a Bax-channel inhibitor also regulated the autophagy pathway. I focused on vacuolin-1 (Fig. 1) since its target molecule has remained unknown. Vacuolin-1 was discovered by image-based screening [59], and recently, Lu et al. has reported that vacuolin-1 is a potent inhibitor of autophagy [60].

Vacuolin-1 inhibits PIKfyve kinase as well as YM201636 does

To identify a vacuolin-1 target molecule, I calculated Rp values (activity versus activity) between vacuolin-1 and the other hit compounds (Table 3). Intriguingly, despite the low number of structural similarities, our hierarchical clustering and Rp analysis strongly suggested that vacuolin-1 had similar biological activity as YM201636 (Fig. 1), which is a potent inhibitor of the phosphatidylinositol phosphate kinase PIKfyve [61]. Moreover, YM201636 is also a potent inhibitor of autophagy [62]. To validate our cluster analysis, I measured the binding activity of vacuolin-1 and YM201636 with PIKfyve using a cell-free binding competition assay. I found that vacuolin-1 and YM201636 were potent binders of PIKfyve, with *Kd* values of 32 and 9 nM, respectively (Fig. 4A). As the assay utilizes an active site-directed ligand as the binding probe, which binds to the ATP site

of PIKfyve, vacuolin-1 is also expected to inhibit PIKfyve in an ATP-competitive manner. Vacuolin-1 might affect autophagy by inhibiting cellular activity of PIKfyve. I therefore performed siRNA experiments to validate whether loss of PIKfyve function induces the formation of cellular giant vacuoles. HeLa cells were treated with three individual siRNAs against PIKfyve for 48 h. Transcription of PIKfyve mRNA was suppressed to <30% of the level in control siRNA-transfected cells (Fig. 4B). In this condition, giant vacuole formation was induced in cells treated with each PIKfyve siRNA (Fig. 4C). Coincidently, giant vacuole formation was also seen in cells treated with vacuolin-1 or YM201636 for 24 h (Fig. 4C).

Vacuolin-1 and YM201636 are late-stage autophagy inhibitors

The results of binding assays against PIKfyve and siRNA against PIKfyve revealed that vacuolin-1 and YM201636 induce giant vacuole formation via PIKfyve inhibition. I further examined the effect of these two compounds against lysosomal protein degradation pathways more precisely. First, I confirmed the effect of compounds against autophagy pathway by Western blotting that detected the conversion ratio of LC3-I to LC3-II in the presence or absence of lysosomal protease inhibitors. This method is more widely accepted to monitor autophagy flux [63]. Treatment with vacuolin-1 or

YM201636 increased LC3-II levels compared with findings in DMSO-treated cells in the absence of protease inhibitors, whereas, in the presence of protease inhibitors, vacuolin-1-treated cells displayed abnormal accumulation of LC3-II as well as DMSO-treated cells did since progression of autophagy was strongly suppressed by the protease inhibitor treatment (Fig. 5A). In addition, I also examined the status of autophagy using an mCherry-AcGFP tandem LC3 assay [64]. This assay is based on the nature of fluorecent protein that GFP-LC3 signals disappeared within the acidic lysosomal condition due to its pKa profile, while mCherry LC3 signals maintained even within the acidic lysosomal condition. In the case of autophagy inhibition, both GFP-signals and mCherry signals are detected, and on the other hand, in the case of autophagy induction, GFP-signals are declined and only mCherry signals are detected. By using this assay, treatment with vacuolin-1 or YM201636 induced the accumulation of AcGFP- and mCherry-positive puncta (Fig. 5B), indicating that vacuolin-1 and YM201636 decreased autophagy flux. These results suggested that vacuolin-1 and YM201636 suppressed autophagy activity probably by inhibiting degradation step of autophagosome.

Next, I analysed the effects of the compounds on the lysosomal maturation pathway. I first monitored the trafficking of the lysosomal enzyme cathepsin D. The processing of

cathepsin D from the precursor to its mature form occurs in lysosomes after it has been transported there via endosomal trafficking. I performed Western blotting, which could detect the band shift of immature and mature cathepsin D to test lysosomal function. Treatment with vacuolin-1 and YM201636 decreased mature cathepsin D levels and increased immature cathepsin D levels, suggesting the possibility that both compounds impaired the endosomal trafficking of *de novo* synthesized lysosomal enzymes, which in turn resulted in the suppression of the lysosomal degradation pathway (Fig. 5C). To examine the possibility, I confirmed the effect of these compounds on protein transport from Golgi bodies to lysosomes. I performed immunostaining of M6PR, a marker of transport between Golgi bodies and lysosomes, and revealed that vacuolin-1 and YM201636 treatment induced enlarged M6PR-positive vesicle formation (Fig. 5D). This result indicated that vacuolin-1 and YM201636 affected the delivery pathway of lysosomal enzymes from Golgi bodies to lysosomes. Both vacuolin-1 and YM201636 probably inhibit autophagy by suppressing the maturation of lysosomes.

In conclusion, I established an assay that can visualize the final step of autophagy and obtained several classes of hit compounds. Subsequent analysis using cellular morphological information revealed for the first time that vacuolin-1 is a potent inhibitor of PIKfyve. My findings suggest that the PIKfyve inhibitors, vacuolin-1 and

YM201636, are novel and useful chemical tools as inhibitor of autophagy and lysosomal maturation. Moreover, because parameters used in my cluster analysis are calculated only from images obtained by primary screening without any additional experiment, morphology-based cluster analysis described in this study is a simple and straightforward approach. Therefore, it will be widely applicable for phenotypic drug discovery and subsequent target identification processes.

Figures and Tables

Figure 1. Compounds used in this study

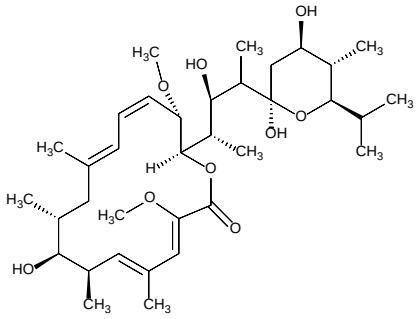

Bafilomycin A1

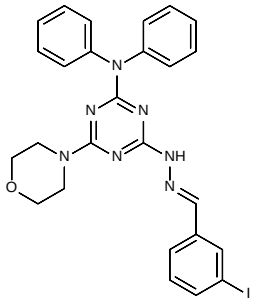

vacuolin-1

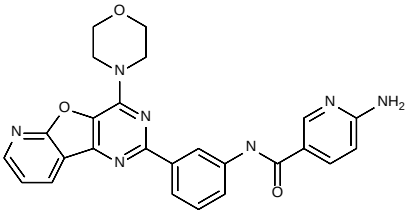

YM-201636

Figure 2. Effect of bafilomycin A1 on autophagy and endocytic pathways. (A) HeLa cells were treated with 100 nM bafilomycin A1 for the indicated times, fixed, and immunostained with LC3, p62, rab7, and LAMP2 antibodies. Representative images are shown. (B) Fluorescent intensity of each parameter was quantified using the IN Cell Developer Toolbox. Values are reported as the mean ± s.e.m. in arbitrary units (n = 4).

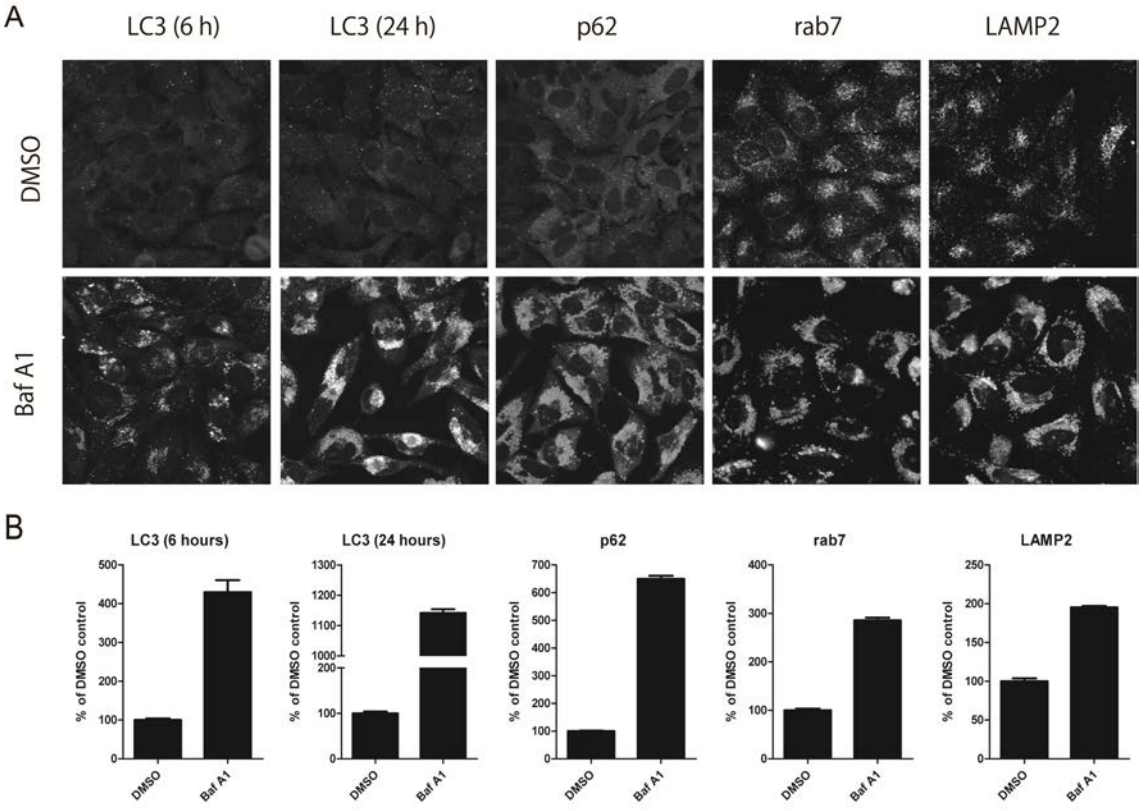
A
LC3 (6 h)
LC3 (24 h)
p62
rab7
LAMP2
DMSO
Baf A1
B
LC3 (6 hours)
LC3 (24 hours)
p62
rab7
LAMP2
% of DMSO control
DMSO
Baf A1

Figure 3. Cluster analysis of hit compounds. (A) Representative parameters calculated from primary screening data. (B) The hit compounds were clustered using morphological parameters. The heat map was visualized using TIBCO Spotfire software for cluster analysis.

A

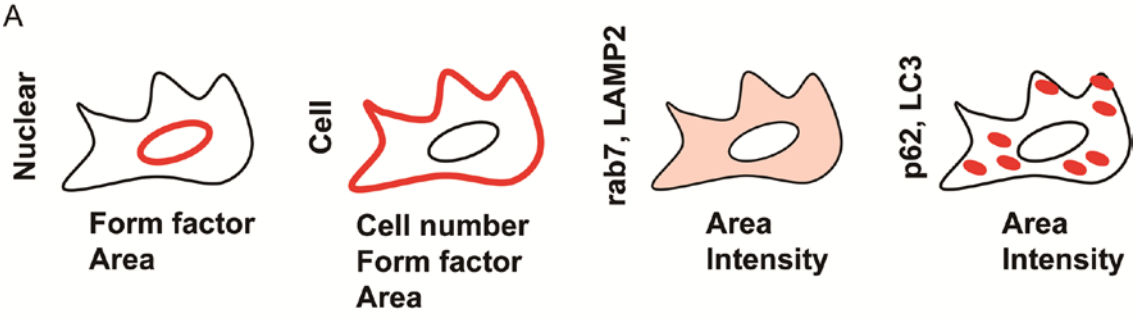
Nuclear
Form factor
Area
Cell
Cell number
Form factor
Area
rab7, LAMP2
Area
Intensity
p62, LC3
Area
Intensity

B

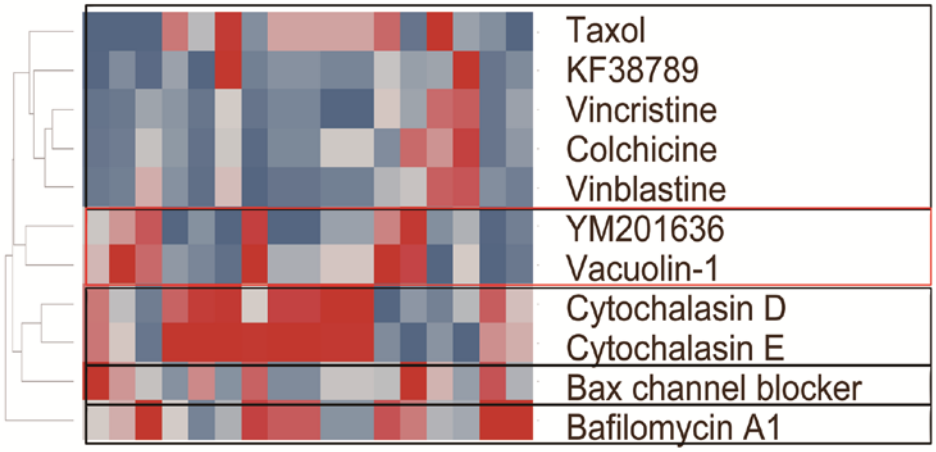
Taxol
KF38789
Vincristine
Colchicine
Vinblastine
YM201636
Vacuolin-1
Cytochalasin D
Cytochalasin E
Bax channel blocker
Bafilomycin A1

Figure 4. Vacuolin-1 and YM201636 inhibit PIKfyve. (A) Vacuolin-1 and YM201636 were evaluated in binding competition assays against PIKfyve. (B) HeLa cells were treated with 30 nM siRNA against PIKfyve for 48 h, and mRNA was extracted to quantify the silencing efficiency of siRNA against PIKfyve by RT-PCR. (C) HeLa cells were treated with 3 μM vacuolin-1 and YM201636 for 24 h. An image was obtained via optical microscopy. (C) HeLa cells were treated with 30 nM siRNA against PIKfyve for 72 h. An image was obtained via optical microscopy.

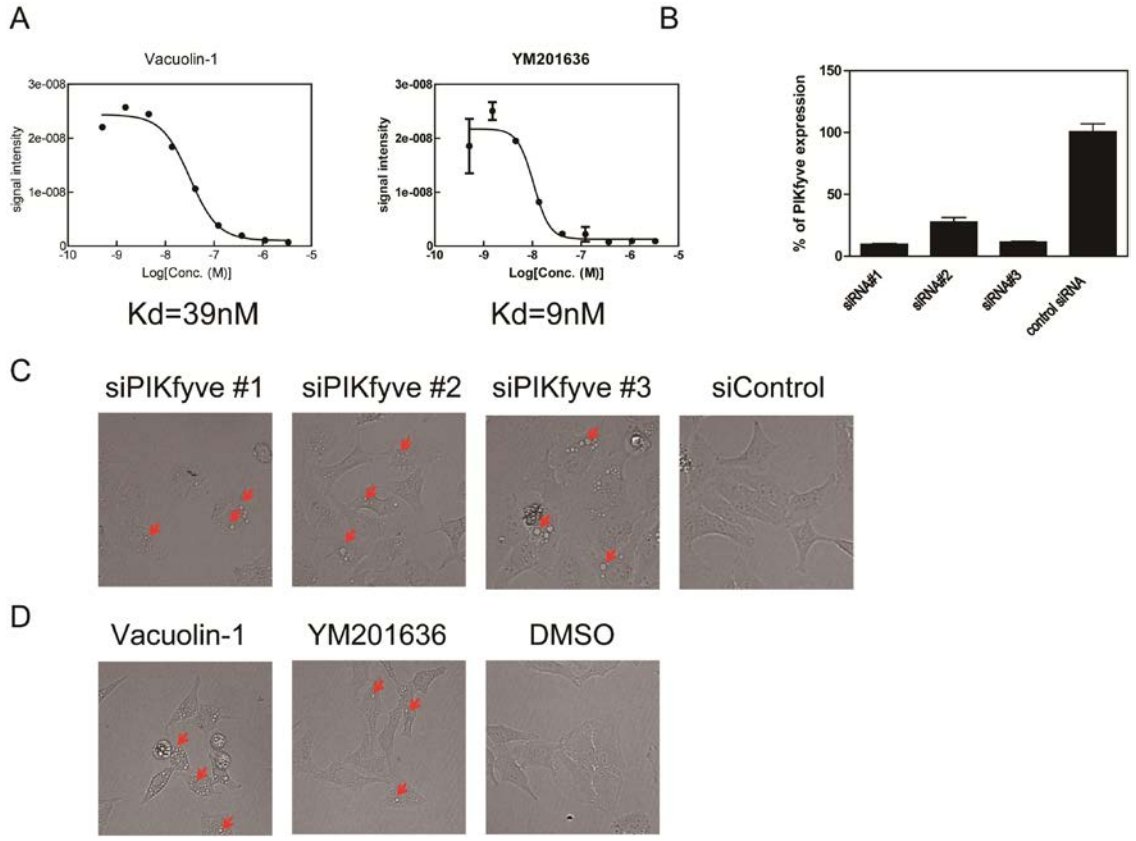
A
Vacuolin-1
signal intensity
Log[Conc. (M)]
Kd=39nM
YM201636
signal intensity
Log[Conc. (M)]
Kd=9nM
B
% of PIKfyve expression
siRNA#1
siRNA#2
siRNA#3
control siRNA
C
siPIKfyve #1
siPIKfyve #2
siPIKfyve #3
siControl
D
Vacuolin-1
YM201636
DMSO

Figure 5. Validation study for vacuolin-1 and YM201636. (A) HeLa cells were treated with 3 μM vacuolin-1 or YM201636 in the presence or absence of the lysosomal protease inhibitor E64d (10 μg/mL) and pepstatin A (10 μg/mL). After 24 h of treatment, cell lysates (10 μg) were separated by 10% polyacrylamide gel electrophoresis, and LC3 was detected by immunoblotting. (B) H4 cells expressing mCherry-GFP LC3 were treated with 3 μM vacuolin-1 and 3 μM YM201636 for 24 h and fixed. Nuclei were stained with Hoechst 33342. (C) HeLa cells were treated with 3 μM vacuolin-1 or YM201636 for 24 h. Cell lysates (10 μg) were separated by 4–20% polyacrylamide gel electrophoresis, and cathepsin D was detected by immunoblotting. (D) HeLa cells were treated with 3 μM vacuolin-1 or YM201636. After 24 h of treatment, cells were fixed and immunostained with M6PR antibody.

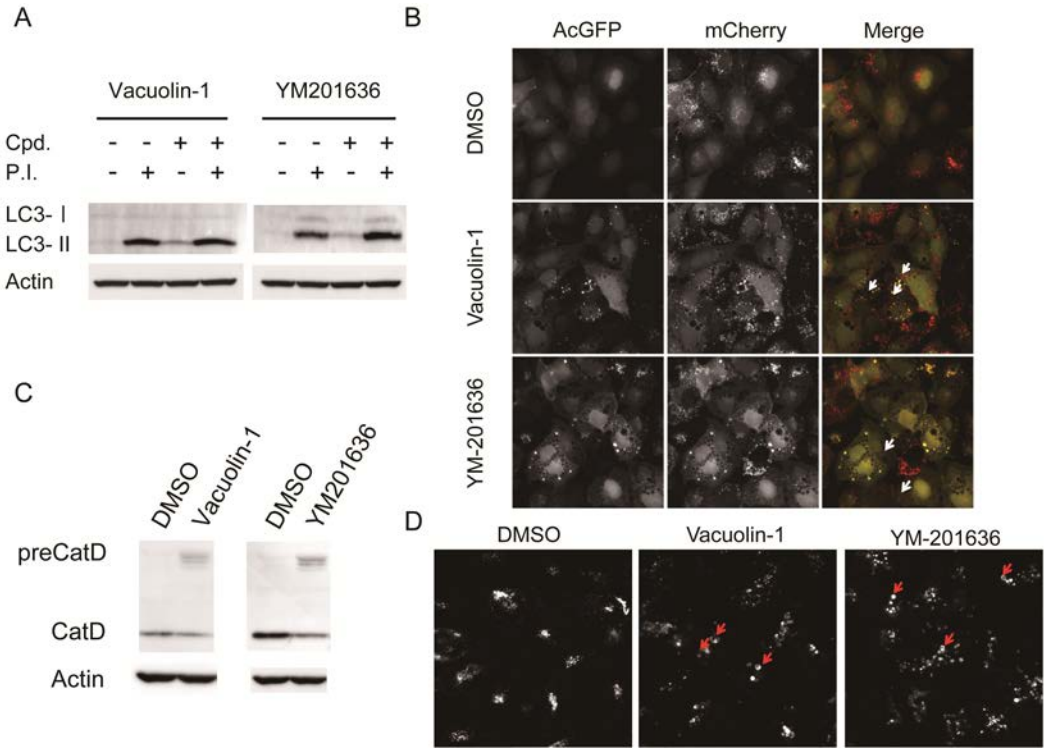
A
Vacuolin-1
YM201636
Cpd.
P.I.
LC3- I
LC3- II
Actin
B
AcGFP
mCherry
Merge
DMSO
Vacuolin-1
YM-201636
C
DMSO
Vacuolin-1
DMSO
YM201636
preCatD
CatD
Actin
D
DMSO
Vacuolin-1
YM-201636

Figure 6. Assay principle of PIKfyve binding assay

Assay principle of binding assay is illustrated by DiscoverX and cited from DiscoverX homepage.

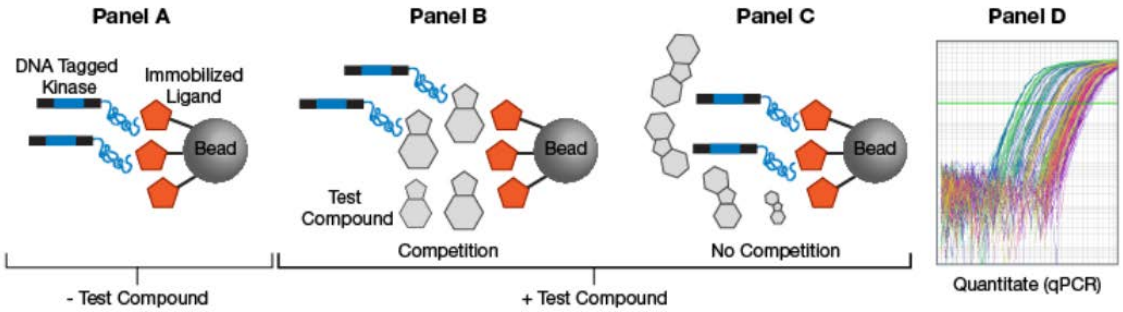
Panel A
Panel B
Panel C
Panel D
DNA Tagged Kinase
Immobilized Ligand
Bead
Test Compound
Competition
No Competition
- Test Compound
+ Test Compound
Quantitate (qPCR)

Table 1

List of hit compounds from the screening.

Compound Name	MOA	Target molecule	Supplier
Taxol	stabilizer of microtubules	tubulin	Tocris
KF 38789	inhibitor of P-selectin-mediated cell-adhesion	tubulin	Tocris
Vincristine	disruptor of microtubules	tubulin	Tocris
Colchicine	disruptor of microtubules	tubulin	Tocris
Vinblastine	disruptor of microtubules	tubulin	Tocris
YM 201636	PIKfyve inhibitor	PIKfyve	Selleck
Vacuolin-1	inducer of vacuolar formation	unknown	Tocris
Cytochalasin D	disruptor of actin polymer	actin	Tocris
Cytochalasin E	disruptor of actin polymer	actin	Millipore
Bax channel blocker (#2160)	inhibitor of cytochrome c release	Bax channel	Tocris
Bafilomycin A1	vATPase inhibitor	vATPase	Millipore

Table 2

List of calculated parameters

Parameter	**Treatment time**	**Antibody**
Nuclear area	6 h	Hoechst33258
Nuclear form factor	6 h	Hoechst33258
Cell count	6 h	Hoechst33258
Cell area	6 h	Hoechst33258
Cell form factor	6 h	Hoechst33258
Nuclear area	24 h	Hoechst33258
Nuclear form factor	24 h	Hoechst33258
Cell count	24 h	Hoechst33258
Cell area	24 h	Hoechst33258
Cell form factor	24 h	Hoechst33258
LC3 intensity	6 h	LC3
LC3 intensity	24 h	LC3
p62 intensity	24 h	p62
rab7 intensity	24 h	Rab7
rab7 area	24 h	Rab7
LAMP2 area	24 h	LAMP2
LAMP2 intensity	24 h	LAMP2

Table 3

The Tanimoto structural similarity indices and Pearson's correlation coefficients (activity versus activity) were calculated for vacuolin-1.

Compound Name	Pearson	Tanimoto
Vacuolin-1	1.00	1.00
YM 201636	0.97	0.25
Cytochalasin E	0.85	0.16
Bafilomycin A1	0.84	0.11
Cytochalasin D	0.84	0.15
Vinblastine	0.57	0.15
Colchicine	0.55	0.16
Vincristine	0.47	0.15
Bax channel blocker (#2160)	0.42	0.20
KF 38789	0.21	0.18
Taxol	0.15	0.16

Chapter Ⅱ

Using a biologically annotated library to analyze the anti-cancer mechanism of serine palmitoyl transferase (SPT) inhibitors

Abstract

Lung cancer is by far the leading cause of cancer death among both men and women. Here, I reveal that inhibition of serine palmitoyl transferase (SPT), the rate-limiting enzyme in sphingolipid synthesis, induced cell death in a lung cancer cell line via a necrosis-dependent pathway. To elucidate the mechanism of cell death induced by SPT inhibition, a biologically annotated library of diverse compounds was screened with an SPT inhibitor. This analysis identified suppressors of SPT inhibitor-mediated cell death. Further analysis using hit compounds from this screening revealed that SPT inhibitors leaded to necrosis-dependent cell death by inducing COX-2 expression. SPT inhibitors might therefore represent novel candidates for cancer therapy via necrosis pathway regulation. My data illustrates that compound combination screening of biologically annotated libraries could be used for mechanism of action of anti-cancer drug.

Introduction

Cancer is a major public health problem worldwide, and accordingly, pharmaceutical companies aim to develop novel anti-cancer-related drugs. Although both genetic and environmental factors are closely related to cancer development and are responsible for some portion of cancer progression, many as yet uncharacterized factors are also involved in cancer progression. In addition to conventional medical and radiation treatments, molecular targeted therapy has recently become popular in the drug discovery process. Especially, developing anti-cancer drugs regulating metabolic pathways that are selectively activated in cancer cells represent a new promising approach to cancer therapy.

Cancer metabolism is the focus of current and emerging therapeutic approaches to anti-cancer drug discovery [65-67]. The best known example of a metabolic shift in cancer cells is the Warburg effect [68]. Cancer cells tend to depend on the glycolytic pathway rather than the tricarboxylic acid (TCA) cycle in order to generate energy more efficiently in a hypoxic microenvironment. Recent metabolomics technology research has revealed additional metabolic pathways that are closely related to cancer cell growth. Newly identified cancer-metabolism-related targets, such as isocitrate dehydrogenase 1 (IDH1) and HMG-CoA reductase, are now considered promising

anti-cancer drug targets [69, 70].

Serine palmitoyl transferase (SPT) mediates the conjugation of serine and palmitoyl CoA to form ceramide and represents a rate-limiting step in sphingolipid synthesis. Ceramide is a well-known lipid that under normal conditions, is readily transferred from the endoplasmic reticulum (ER) to the Golgi by the ceramide transfer protein CERT, where it undergoes further synthesis to glucosylceramide, sphingomyelin, and sphingosine-1-phosphate [71, 72]. Abnormal sphingolipid metabolism has been observed in several types of cancer cells. In head and neck cancer, ceramidase overexpression is occurred, which enhances resistance to Fas ligand mediated apoptosis. In addition, in various solid cancers, sphingosine kinase 1 overexpression is occurred, which leads to enhanced proliferation [73-75].

Although the metabolomics approach to cancer drug discovery works well and has led to the identification of new anti-cancer drug targets, the relationship between metabolic alterations and cancer cell growth is not always clear. Therefore, it is important for drug discovery researchers to understand the mechanisms of action (MOA) for such drugs. There are two commonly accepted methods for analyzing the MOA of cancer drugs. One method involves a target specific hypothesis-based approach that combines known information with newly obtained data from analyses such as

transcriptome and metabolome. The other method involves a discovery-based approach involving a functional genomics analysis of whole genome siRNA or shRNA [76, 77]. Functional genomics analyses have provided many novel possibilities with regard to target relationships and thus represent a powerful approach for the identification of relatively novel targets. However, these unbiased siRNA- or shRNA-based approaches share the fundamental challenges of off-target effect [27, 28], knockdown efficiency, protein turnover, and compensatory reactions [78]. The establishment of alternative methods would be valuable to my understanding of the MOA of anti-cancer drugs.

Biologically annotated library screening is currently attracting considerable interest as a straightforward approach to phenotypic drug discovery [79-84]. This approach allows me to easily link target molecules with disease phenotypes and to generate hypotheses regarding the underlying biological mechanisms. Unlike siRNA or shRNA, small molecules are directly inhibit or activate target protein, independent from expression level and turnover rate of target protein. Moreover, it is noteworthy that tool compounds collected in biologically annotated library are optimized to enhance not only the potency against target protein but also target selectivity. Therefore, I hypothesized that MOA analysis of anti-cancer drugs by using biologically annotated library could become complementary methods for functional genomics.

In this study, I experimentally demonstrated that inhibitory compounds for SPT, the rate-limiting enzyme in sphingolipid synthesis, inhibited the growth of lung cancer cells depending on their inhibitory activity. In addition, I also investigated the MOA of SPT inhibitors by screening a biologically annotated library and successfully isolated a compound that was able to cancel the anti-cancer activity of SPT inhibitors. As a result, I demonstrated that COX-2 pathway played essential role in the anti-cancer activity of SPT inhibitors.

Materials and Methods

Materials

Reagents were obtained from Life Technologies (Carlsbad, CA, USA) unless otherwise specified. Anti-COX2 antibody (#12282, used at 1/1000 dilution for western blotting) and anti-actin antibody (#4970, used at 1/1000 dilution for western blotting) were purchased from Cell Signaling Technologies (Danvers, MA, USA). Z-vad, caspase 3/7 Glo reagent, and ROS Glo reagent were purchased from Promega Corp (Fitchburg, WI, USA). Ferrostatin-1 was purchased from SIGMA (St. Louis, MO, USA).

Compounds

Biologically annotated compounds were collected to create a screening compound library. SPT inhibitors were synthesized at Takeda Pharmaceutical Company, Ltd. (Fujisawa, Japan) [85].

Preparation of human SPT2 enzyme

Polymerase chain reaction (PCR) with specific primers was used to generate cDNA encoding human SPT2, and the PCR product was subsequently subcloned to generate expression vectors. For preparation of the SPT2 enzyme, FreeStyle293 cells were

transfected with human SPT2 expression plasmids and cultured for three days. Cells were then homogenized in 50 mM HEPES buffer (pH 7.5) containing 250 mM sucrose, 5 mM EDTA, 5 mM DTT, and Complete, EDTA-free (Roche Applied Science, Penzberg, Upper Bavaria, Germany). Cell homogenates were centrifuged, and supernatants were harvested. Total membrane fractions were isolated by ultracentrifugation. Pellets were re-suspended in 50 mM HEPES buffer (pH 7.5) containing 5 mM EDTA, 5 mM DTT, and Complete, EDTA-free (Roche) and stored at −80°C. The protein concentration was determined with using the CBB Protein Assay [86].

Enzyme assay

Enzyme reactions were run in 20 µL volumes with assay buffer comprising 100 mM HEPES (pH 8.0), 2.5 mM EDTA, 5 mM DTT, and 0.01% bovine serum albumin (fatty acid-free), and conducted in a 384-well assay plate. Briefly, 5 µL of a tested compound and 10 µL of 100 µg/mL SPT2-expressed-membrane dissolved in assay buffer were mixed and incubated for 60 minutes. Subsequently, 5 µL of a substrate solution containing 2 mM L-serine and 20 µM palmitoyl-CoA in assay buffer were added to start the enzyme reaction. After a 15-minute incubation at room temperature, the reaction was terminated by adding 20 µL of 2% formic acid. Finally, 40 µL of acetonitrile

containing 600 nM C17-sphinganine were added as an internal standard.

High-throughput online solid-phase extraction was performed using a RapidFire® 300 device (Agilent Technologies, Santa Clara, CA, USA). Mass spectrometric analysis was performed using an API-4000™ triple quadrupole mass spectrometer (AB SCIEX, Framingham, MA, USA) in positive SRM mode. The SRM transitions for 3-ketodihydrosphingosine (reaction product) and C17-sphinganine were set to 300.5/270.3 and 288.4/60.2, respectively. Analytical data were acquired using Analyst software, version 1.5.0 (AB SCIEX), and measured value of 300.5/270.3 was divided by that of 288.4/60.2 for calibration. The IC_{50} values for test compounds were calculated using XLfit software (IDBS, London, UK).

Cell line

HCC4006 cells were purchased from ATCC (Manassas, VA, USA) and maintained in RPMI supplemented with 10% fetal bovine serum (Corning Corp., Midland, MI, USA).

Growth inhibition assay

HCC4006 cells were dispensed into a 384-well culture plate at a density of 250 cells/well in 40 μL of culture medium and cultured overnight. Subsequently, the cells were treated

with 10 μL of a tested compound and cultured for five days. The medium was then removed and replaced with 30 μL of CellTiter Glo Luminescent Cell Viability Assay reagent (Promega, Fitchburg, WI, USA). Luminescence was measured on an EnVision device (PerkinElmer, Waltham, MA, USA). The IC_{50} values for test compounds were calculated using GraphPad Prism 5.0.

Lactate dehydrogenase (LDH) release

HCC4006 cells were seeded in black 384-well plates and treated with compounds for 96 hours. From each well, 20 μL of cell culture medium was transferred to a 384-well clear-bottomed plate (#3680, Corning Corp.); CytoTox 96 Non-Radioactive Cytotoxicity Assay (Promega Corp.) reagent was added to each well, followed by a 30 minute incubation; cell variability was measured on a Spectramax Paradigm multiplate reader (Molecular Device Corp., Sunnyvale, CA, USA).

Caspase 3/7 assay

HCC4006 cells were seeded in white 384-well plates (#3570, Corning Corp., Corning, NY, USA) and treated with the indicated compounds for 96 hours. Caspase 3/7 Glo (Promega Corp.) was added to each well, and cell viability was determined by measuring the

firefly luciferase intensity on an EnVision device (PerkinElmer, Waltham, MA, USA).

ROS Glo assay

HCC4006 cells were seeded in white 384-well plates (#3570, Corning Corp.) and treated with the indicated compounds for 96 hours. ROS-Glo (Promega Corp.) substrate was added to each well, after which cells were incubated at 37ºC for three hours. Detection solution was then added to each well, and reactive oxygen species (ROS) generation was determined by measuring the firefly luciferase intensity on an EnVision device.

siRNA transfection

HCC4006 cells were transfected with a final concentration of 6 nM siRNA. RNAiMAX was used for the reverse transfection according to the manufacturer's instructions. To silence COX-2 or MAGL, specific siRNAs (Silencer® Select Pre-designed siRNA from Life Technologies; s11472, s11473, and s11474 for COX-2, s22379, s22380, and s22381 for MAGL, and negative control siRNA #1 for control) were used. Forty-eight hours after siRNA transfection, cells were harvested for real-time RT-PCR analysis using 1-step cells to CT reagent, and the knockdown of each mRNA was confirmed using TaqMan probes (Hs00228159_m1 for COX-2, Hs00996004_m1 for MAGL, and Hs01060665_g1

for Actin as an internal control).

Monoacylglycerol lipase (MAGL) assay

Compounds were dissolved in DMSO and subsequently diluted in enzyme reaction buffer (10 mM Tris-HCl, pH 7.5, 1 mM EGTA, 0.025% (w/v) Triton X-100, 0.01% bovine serum albumin [BSA]). Recombinant human MAGL was diluted in enzyme reaction buffer to a concentration of 7.5 ng/mL. Five microliters of compound solution were added to each well of a 384-well assay plate, and 5 µL of enzyme mixture were added per well. The mixtures were incubated at room temperature for 60 min. Next, 5 µL of substrate solution (150 µM 2-arachidonylglycerol) was added to each well, and the mixture was incubated at room temperature for 10 min. The reaction was stopped by adding 10 µL of 2% formic acid and 50 µL of acetonitrile containing 3 µM arachidonic acid-d8 (Cayman Chemical). Arachidonic acid production was detected via RapidFire mass spectrometry and corrected to arachidonic acid-d8.

Combination screening

HCC4006 cells were seeded in black 384-well plates and pretreated with Biologically annotated compounds for 1 hour, after which SPT inhibitors were added for 120 hours.

CellTiter Glo was added to each well, and cell variability was determined by measuring the firefly luciferase intensity on an EnVision device.

Western blotting

Cells were collected and lysed in RIPA buffer (Wako Pure Chemicals, Osaka, Japan) containing protease inhibitor cocktail (Roche, Basel, Switzerland). Lysates was boiled with sodium dodecyl sulfate (SDS) sample buffer (Bio-Rad, Hercules, CA, USA) containing 100 μM of dithiothreitol. Samples were electrophoresed on 5%–20% SDS polyacrylamide gels (ATTO, Tokyo, Japan), transferred to polyvinylidene fluoride membranes using an iBLOT apparatus (Thermo Fisher Scientific, Waltham, MA, USA), and immunostained using the indicated antibodies.

Pathway enrichment analysis

I used the Ingenuity Pathway Analysis (IPA) system for canonical pathway enrichment analysis to perform functional enrichment tests of target candidate genes linked to the hit compounds.

Statistical analysis

Values are presented as means ± standard deviations. Statistical significance among groups was determined using an analysis of variance (ANOVA) followed by Dunnett's test. A P value <0.05 was considered statistically significant.

Curve Fitting

Curve fitting has performed by using GraphPad Prism 6.0 software (Prism).

Following equation was used;

a. For cell growth inhibitory activity

Y=Bottom + (Top-Bottom)/(1+10^((X-LogIC50)))

Bottom was fixed to 100

b. For other assay

Y=Bottom + (Top-Bottom)/(1+10^((LogEC50-X)))

Bottom was fix to 100

Results and Discussion

SPT inhibitors attenuate lung cancer cell growth

Previous studies suggested that SPT inhibition suppressed the growth of both melanoma and lung cancer cells [87, 88]. I found that the lung cancer cell line HCC4006 was sensitive to myriocin, a known SPT inhibitor (Fig. 1A). Therefore, I synthesized 137 pyrazolopyridine derivatives as SPT inhibitors and used these to validate the relationship between *in vitro* SPT activity inhibition and cancer cell growth. I confirmed that the inhibition of HCC4006 cancer cell growth correlated well ($R^2 = 0.87$) with the *in vitro* inhibition of SPT2 enzyme activity, suggesting that SPT inhibition is responsible for HCC4006 cancer cell growth inhibition (Fig. 1B). One of the pyrazolopyridine derivatives, tentatively called “compound 1”, inhibited SPT2 with an IC_{50} value of 0.8 nM in an *in vitro* enzyme assay and suppressed HCC4006 cell growth with an IC_{50} value of 59 nM (Fig. 1C). From then on, I utilized compound 1 as a chemical probe against SPT.

SPT inhibitor induces necrosis-dependent cell death in HCC4006 cells

Although SPT inhibition was shown to induce growth inhibition in HCC4006 cancer cells, the underlying MOA remained unclear. The cell growth inhibition might be caused

as the result of cell death. Cell death can be largely classified as follows, according to morphological and biochemical characteristics; apoptosis or programmed cell death, non-apoptotic cell death such as necrosis, and ferroptosis, a recently found well-regulated cell death mechanism [89, 90]. To understand the MOA of compound 1, I examined which types of cell death were induced by it using a well-characterized assay system and specific inhibitors against each cell signaling and metabolic pathways. First, I tested the apoptotic pathway since SPT inhibition induced apoptotic signals [88]. However, under my assay conditions, I found that caspase 3/7 cleavage, a phenotypic marker of apoptosis, was activated by compound 1 only at concentrations exceeding 3 μM. Moreover, cells treated with another SPT inhibitor, myriocin, used as a control compound, did not cause apoptosis. Therefore, the caspase 3/7-activation observed only at high concentrations of compound 1 might be the result of an off-target effect (Fig. 2A). I also confirmed that treatment with the pan-caspase inhibitor, z-vad, did not attenuate SPT inhibitor-induced growth inhibition (Fig. 2B). Taken together, these observations suggested that apoptosis was unlikely to be involved in the SPT inhibitor-dependent cell growth inhibition. Second, I examined whether SPT inhibitor treatment would induce ferroptosis. Ferroptosis is a newly identified type of cell death involving the iron dependent accumulation of reactive lipid species [91]. I tested that treatment with SPT

inhibitors induced the generation of reactive oxygen species (ROS), a hallmark of ferroptosis. Treatment with compound 1 and myriocin induced ROS production in a dose-dependent manner, However, treatment with ferrostatin-1, a well-characterized ferroptosis inhibitor, did not attenuate compound 1-induced cell growth inhibition (Fig. 2D). These data suggest that ROS generation is a secondary effect of SPT inhibitor treatment and that SPT inhibitor-induced cell growth inhibition is independent of ferroptosis. Third, I evaluated whether SPT inhibitor treatment would induce necrosis. Necrosis is an apoptosis independent cell death mechanism characterized by a disruption of the cell membrane structure and subsequent release of cellular components to the extracellular medium [92]. Treatment with compound 1 and myriocin induced LDH release in a dose-dependent manner with respective EC_{50} values of 47 nM and 0.4 nM (Fig. 3A), indicating good agreement with the IC_{50} values for inhibitory effect on cell growth (59 nM and 4 nM, respectively). In order to examine whether SPT inhibition leads to necrosis, I further investigated the effect of known necrosis inhibitor IM-54, which was originally identified as a suppressor of hydrogen peroxide induced necrosis [93]. Co-treatment of compound1 or myriocin with IM-54 attenuated compound1 or myriocin induced cell death (Fig. 3B). These results collectively indicate that SPT inhibitors suppress cell growth via the necrotic pathway.

Compound combination screening using a biologically annotated library with SPT inhibitors

A recent study illustrated that functional genomics studies involving siRNA or shRNA could be a useful approach to the elucidation of unknown MOA of targeted compounds [94]. However, suppression of a single gene might be overwhelmed by the compensatory activity of functionally redundant genes [78] and, for siRNA studies in particular, the efficiency of knockdown varied according to the target protein and, in most cases, partial knockdown did not affect the desired phenotype; in addition, off-target effects of siRNA are frequently observed [27, 28]. To overcome these obstacles, I performed an unbiased combination study using a biologically annotated library with SPT inhibitors. Several pharmaceutical companies have proposed the concept of a biologically annotated library to the elucidation of unknown MOA of targeted compounds [79-82]. I collected approximately 3000 compounds to form the biologically annotated library for a phenotypic screening in this study. My criteria for the selection of compounds were *in vitro* pharmacological activity with IC50 or EC50 value of less than or equal to 1 μM on each target protein, which is based on the results of cell-free and cell-based assays with multiple types such as functional and binding assays, as shown in Fig. 4A and Table 1.

Consequently, the biologically annotated compound library targeted approximately 1500 unique proteins, each of which was often annotated by multiple compounds to avoid the misinterpretation of the results caused by off-target effects of small molecules. In fact, 70% of target protein information was annotated by more than one compound. The remaining 30% covered by a single compound for each was still included. In my combination study, the concentration of compound 1 was set to 1 μM, whose concentration is GI_{100} against HCC4006 cells with biologically annotated library compounds at a concentration of 3 μM; the latter was expected to fully regulate the target protein activity. I co-treated 3 μM biologically annotated libraries with or without 1 μM SPT inhibitor (Fig. 4B), and identified 33 hit compounds that mitigated SPT inhibitor induced cell death (Fig. 4C and Table 2).

Upregulation of COX-2 expression triggers necrosis in SPT inhibitor treated cells

Pathway enrichment analysis, using IPA pathway enrichment software, has performed to reveal essential pathways related to SPT inhibitor induced cell death, and eighteen pathways were nominated as candidate pathways (Fig. 4D). I focused on the prostanoid biogenesis pathway because I noticed that 4 of the 33 hit compounds were related to COX-2, which catalyzes the conversion of arachidonic acid to prostanoid. Two selective

COX-2 inhibitors, celecoxib and rutaecapine, were included in this category [95], and were found to dose-dependently attenuate compound 1 mediated growth inhibition (Fig. 5A). COX-2 is an inducible family protein that is expressed at low levels under basal conditions; expression of this protein can be induced by particular stimuli, leading to the generation of prostaglandin products [96, 97]. I examined whether treatment with SPT inhibitors would induce COX-2 expression, thus validating my combination library screening findings, and confirmed that treatment with SPT inhibitors induced COX-2 expression after 96 hours (Fig. 5B). I also confirmed that beclomethasone and flumethasone suppressed SPT inhibitor mediated cell death (Fig. 5C). These two compounds were previously reported as suppressors of COX-2 expression [98]. These results strongly suggested that compound 1 induced cell growth inhibition was mediated by COX-2 function. Next, I re-analyzed the results of my biologically annotated library screening and found that JZL184 suppresses compound 1 induced cell growth inhibition. JZL184 is an irreversible inhibitor for monoacylglycerol lipase (MAGL), the primary enzyme responsible for degrading the endocannabinoid 2-arachidonoylglycerol (2-AG) to arachidonic acid [95]. I measured the inhibitory activities of two other lipase inhibitors, CHEMBL130098 and CEHMBL1082517 against MAGL because arachidonic acid metabolism was likely to key pathway for

compound 1 induced cell growth inhibition. As expected, both compounds inhibited in vitro MAGL enzyme activity (Table 3). These results indicate that seven compounds out of 33 hit compounds identified via combination library screening were related to arachidonic acid metabolism. These observations strongly support the validity of our biologically annotated library screening strategy. Finally, I performed a siRNA-based knock-down experiment to exclude the possibility of off-target effect of annotated compounds. Treatment of COX-2- or MAGL-targeting siRNAs suppressed compound 1 induced cell growth inhibition (Fig. 6), and this result also supported the importance of COX-2 and MAGL related pathway for SPT inhibitor mediated cancer cell death.

In summary, I performed a combination screening of compounds using a biologically annotated library to reveal the MOA of SPT inhibition and found that COX-2 expression was upregulated by SPT inhibition. Although the mechanism by which COX-2 expression was induced remains unclear, COX-2 induction was critical for SPT inhibition-induced cell death (Fig. 5D). My results present the possibility that the expression level of MAGL or COX2 in lung cancer patients could be one of candidate of patient stratification marker. A more detailed analysis will be the subject of further study. Finally, I emphasize that my combination approach involving a biologically annotated library could be widely applicable to the investigation and discovery of the

MOA of other types of anti-cancer drugs. My compound combination screening using biologically annotated library for anti-cancer drug MOA analysis could provide novel findings on target related pathway and be applicable as a complementary method for functional genomics-based MOA analysis.

Figures and Tables

Figure 1. Chemical structure and growth inhibitory activities of serine palmitoyl transferase (SPT) inhibitors.

(A) HCC4006 cells were treated with myriocin for 120 hours. Cell viability was measured using CellTiter Glo. The chemical structure of myriocin is also described. Values are reported as means ± s.e.m. in arbitrary units (n = 4). (B) Relationship of HCC4006 cell growth inhibition with SPT inhibitory activity. HCC4006 cells were treated with a range of doses of SPT inhibitor for 120 hours. The pIC50 values, indicating growth inhibitory activity, of each compound are plotted versus the *in vitro* SPT2 enzyme inhibitory activity. (C) HCC4006 cells were treated with compound 1 for 120 hours. Cell viability was measured by CellTiter Glo. The chemical structure of compound 1 is also described. Values are reported as means ± s.e.m. in arbitrary units (n = 4).

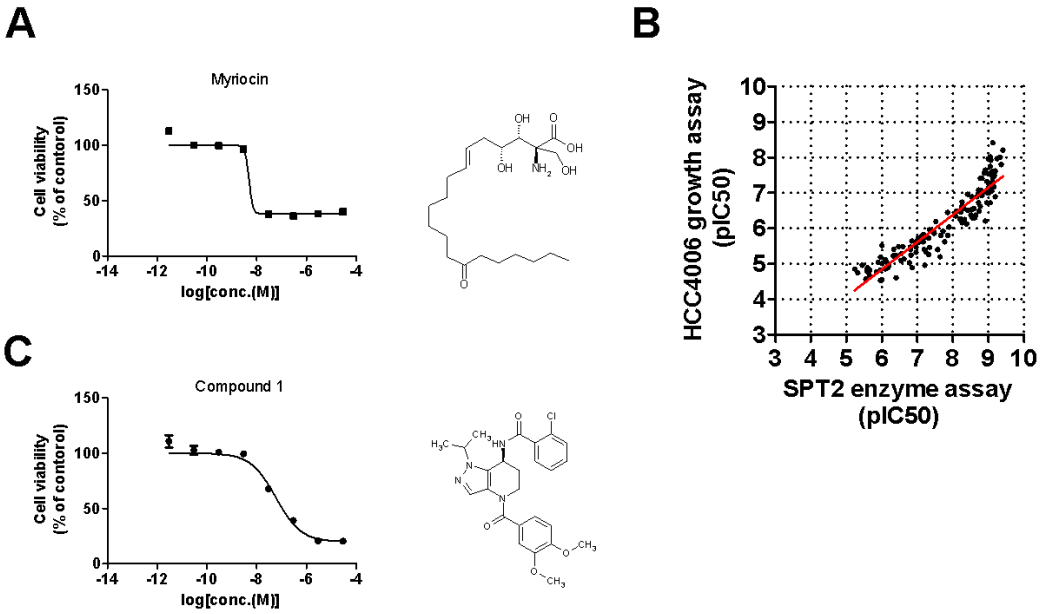
A
Myriocin
Cell viability
(% of contorol)
150
100
50
0
-14
-12
-10
-8
-6
-4
log[conc.(M)]
OH
O
OH
OH
NH2
OH
O
B
HCC4006 growth assay
(pIC50)
10
9
8
7
6
5
4
3
3 4 5 6 7 8 9 10
SPT2 enzyme assay
(pIC50)
C
Compound 1
Cell viability
(% of contorol)
150
100
50
0
-14
-12
-10
-8
-6
-4
log[conc.(M)]
H3C
CH3
HN
O
Cl
N
N
N
O
O
CH3
O
CH3

Figure 2.

(A) HCC4006 cells were treated with various concentrations of compound 1 or myriocin for 96 hours. Caspase 3/7 activity was measured using a Caspase 3/7 Glo assay.

(B) HCC4006 cells were co-treated various concentrations of compound 1 with or without 20 μM z-VAD for 120 hours. Cellular viability was measured using CellTiter Glo.

(C) HCC4006 cells were treated with various concentrations of compound 1 or myriocin for 96 hours. Intracellular reactive oxygen species (ROS) production was measured using a ROS Glo assay.

(D) HCC4006 cells were co-treated various concentrations of compound 1 with or without 10 μM Ferrostatin-1. Cellular viability was measured by CellTiter Glo.

A

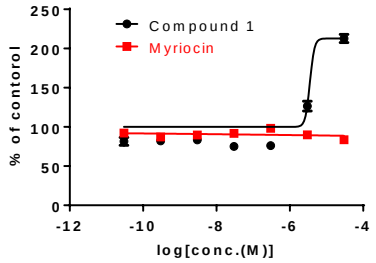
Compound 1
Myriocin
% of contorol
log[conc.(M)]

B

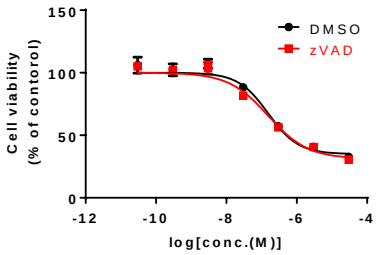
DMSO
zVAD
Cell viability
(% of contorol)
log[conc.(M)]

C

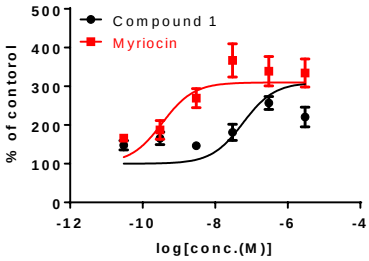
Compound 1
Myriocin
% of contorol
log[conc.(M)]

D

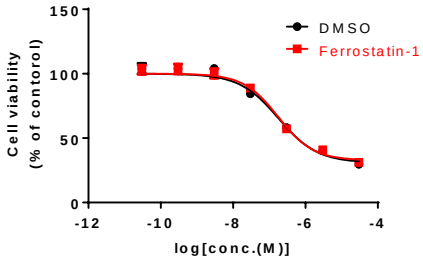
DMSO
Ferrostatin-1
Cell viability
(% of contorol)
log[conc.(M)]

Figure 3. Characterization of the cell death mechanism of action.

(A) HCC4006 cells were treated with various doses of compound 1 for 96 hours. Necrosis activity was measured by a lactate dehydrogenase (LDH) release assay. (B) HCC4006 cells were co-treated with 1 μM compound 1 or 300 nM myriocin and 10 μM necrosis inhibitor IM-51 for 120 hours. Cell viability was measured by CellTiter Glo.

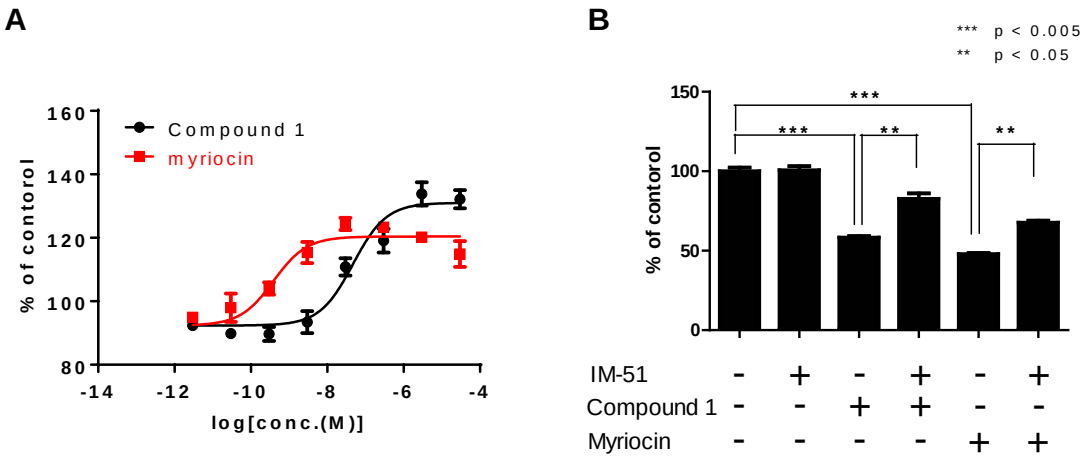
A
B
Compound 1
myriocin
% of contorol
log[conc.(M)]
*** p < 0.005
** p < 0.05
IM-51
Compound 1
Myriocin

Figure 4. Unbiased screening with a biologically annotated library.

(A) Composition of library used for combination screening. (B) Scheme of combination library screening. (C) HCC4006 cells were treated with the biologically annotated library components in the presence or absence of 1 μM compound 1 for 120 hours. The inhibitory activity of each compound is plotted. (D) Results of an IPA software-based pathway enrichment analysis. The significance of canonical pathways was determined by IPA's default threshold.

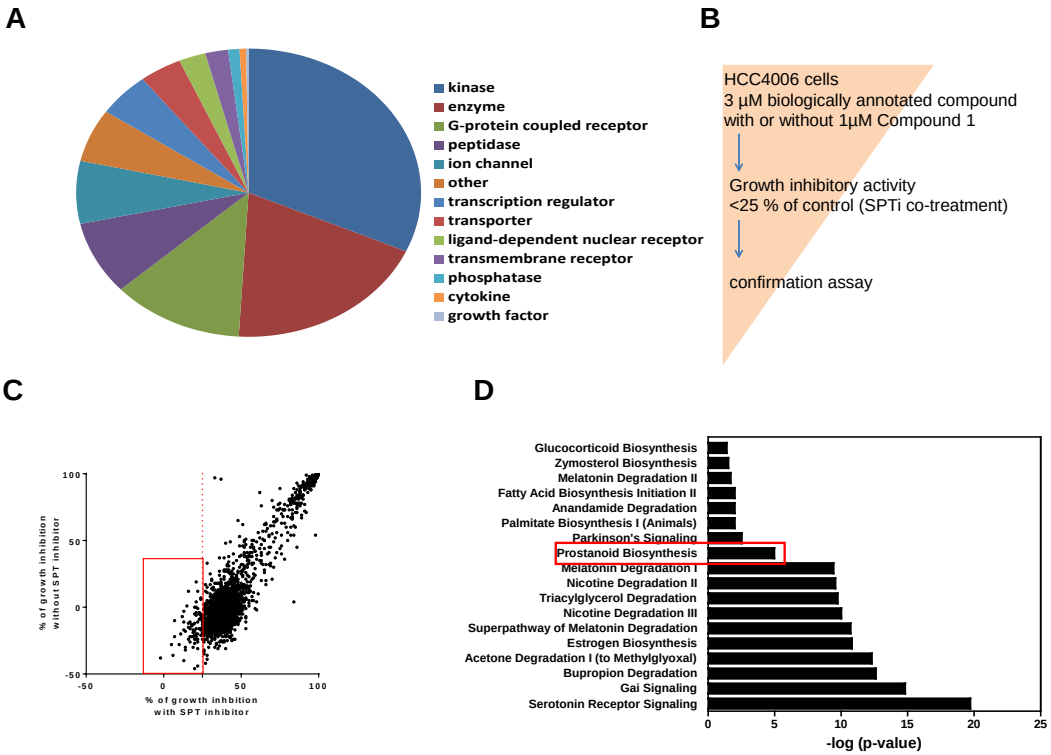
A
kinase
enzyme
G-protein coupled receptor
peptidase
ion channel
other
transcription regulator
transporter
ligand-dependent nuclear receptor
transmembrane receptor
phosphatase
cytokine
growth factor
B
HCC4006 cells
3 µM biologically annotated compound
with or without 1µM Compound 1
Growth inhibitory activity
<25 % of control (SPTi co-treatment)
confirmation assay
C
% of growth inhibition without SPT inhibitor
% of growth inhbition with SPT inhibitor
100
50
0
-50
-50
0
50
100
D
Glucocorticoid Biosynthesis
Zymosterol Biosynthesis
Melatonin Degradation II
Fatty Acid Biosynthesis Initiation II
Anandamide Degradation
Palmitate Biosynthesis I (Animals)
Parkinson's Signaling
Prostanoid Biosynthesis
Melatonin Degradation I
Nicotine Degradation II
Triacylglycerol Degradation
Nicotine Degradation III
Superpathway of Melatonin Degradation
Estrogen Biosynthesis
Acetone Degradation I (to Methylglyoxal)
Bupropion Degradation
Gai Signaling
Serotonin Receptor Signaling
0
5
10
15
20
25
-log (p-value)

Figure 5. Validation of the combination library screening results.

(A) HCC4006 cells were treated with various concentrations of the COX-2 selective inhibitors celecoxib and rutaecapine together with 1 μM compound 1 for 120 hours. Cellular viability was measured with CellTiter Glo. (B) HCC4006 cells were treated with 1 μM compound 1 or 300 nM myriocin for 120 hours. Cell lysates (5 μg) were separated via 4–20% polyacrylamide gel electrophoresis, and COX-2 and beta-actin protein levels were detected via immunoblotting. (C) Cells were treated with various concentrations of COX-2 expression inhibitors, Beclomethasone and Flumethasone, and 1 μM compound 1 for 120 hours. Cellular viability was measured using CellTiter Glo. Values are reported as means ± s.e.m. in arbitrary units (n = 4). (D) Summary of the molecular mechanism of action of SPT inhibitors.

A

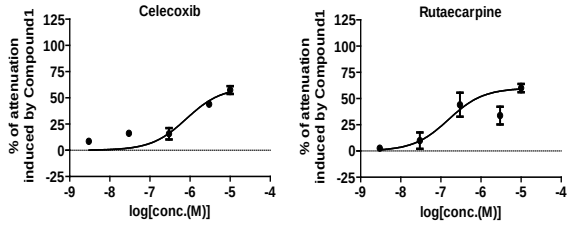
Celecoxib
Rutaecarpine
% of attenuation induced by Compound1
log[conc.(M)]

B

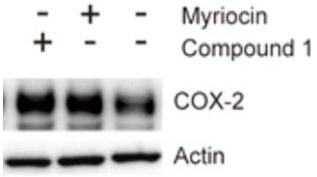
- + - Myriocin
+ - - Compound 1
COX-2
Actin

C

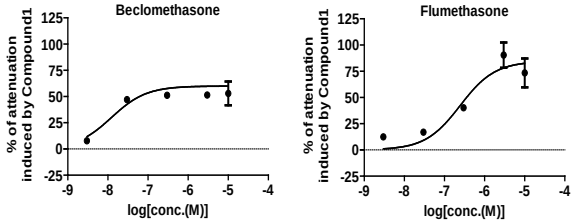
Beclomethasone
Flumethasone
% of attenuation induced by Compound1
log[conc.(M)]

D

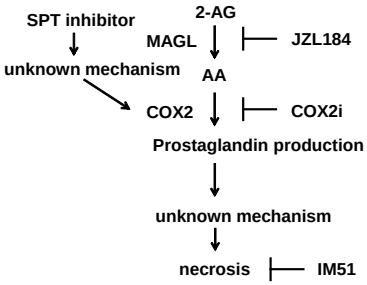
SPT inhibitor
2-AG
MAGL
JZL184
unknown mechanism
AA
COX2
COX2i
Prostaglandin production
unknown mechanism
necrosis
IM51

Figure 6. Validation of the combination library screening results by using siRNAs.

(A) HCC4006 cells were co-treated 6 nM COX-2, MAGL, or control siRNA with 3 μM compound 1 for 72 hours. Cellular viability was measured using CellTiter Glo, and the relative viability compared to DMSO treated cells was shown.

(B) HCC4006 cells were treated with 6 nM COX-2, MAGL or control siRNA for 48 hours. Total transcripts in treated cells were subjected to measure expression level of COX-2 and MAGL by qPCR. Relative knock-down efficiency was calculated by delta-delta CT method.

A

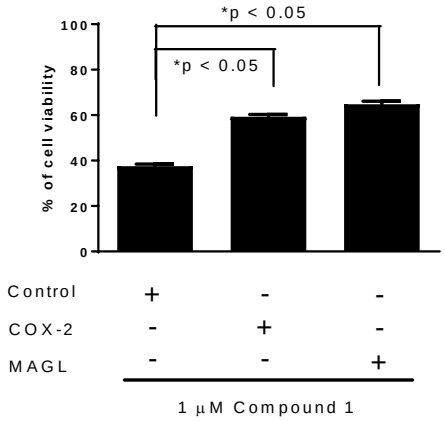
*p < 0.05
*p < 0.05
% of cell viability
100
80
60
40
20
0
Control + - -
COX-2 - + -
MAGL - - +
1 µM Compound 1

B

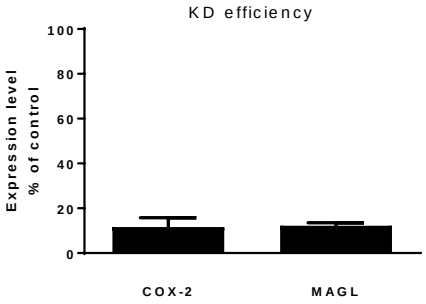
KD efficiency
Expression level
% of control
100
80
60
40
20
0
COX-2
MAGL

Table 1.

Composition of library used for combination screening.

Type(s)	Unique Target
kinase	424
enzyme	318
G-protein coupled receptor	180
ion channel	143
peptidase	112
other	90
transporter	77
transcription regulator	68
transmembrane receptor	37
ligand-dependent nuclear receptor	34
phosphatase	18
cytokine	9
growth factor	5
translation regulator	1
Total	1516

Table 2. List of hit compounds identified via combination screening.

Compound Name	Mechanism of Action	Target class
Orlistat	Arachidonic acid production	Enzyme
CHEMBL130098	Hormone sensitive lipase	Enzyme
CHEMBL1082517	Lysosomal acid lipase (LIPA)	Enzyme
JZL184	Monoacyl glycerol lipase(MAGL)	Enzyme
Flumetasone	COX2	Enzyme
Beclomethasone	COX2	Enzyme
Celecoxib	COX2	Enzyme
Rutaecarpine	COX2	Enzyme
Econazole	Ergosterol synthesis	Enzyme
CHEMBL557129	CDC25B	Enzyme
CHEMBL1471965	PSMD14	Enzyme
Necrostatin-1	RIPK1	Kinase
CHEMBL1462325	AHR	ligand-dependent nuclear receptor
CHEMBL334330	RARB	ligand-dependent nuclear receptor
PRIMA-1	p53	Transcription regulator
pubchem2115839	STAT3	Transcription regulator
CID:|4283428	KLF5	Transcription regulator
CHEMBL165418	ABCC1	Transporter
Bromocryptine	D2R	GPCR
MK-329	CCKAR	GPCR
Loxapine	5HTR	GPCR
N-methylquipazine	5HT3A	GPCR
CP-135807	5-HT1D	GPCR
CHEMBL133534	MT1	GPCR
Promethazine	H1R	GPCR
Tripelennamine	H1R	GPCR
Tolterodine	M2/M3	GPCR
Montelukast	Leukotriene receptor	Transmembrane receptor
4EGI-1	eIF4E/eIF4G interaction inhibitor	Other
Pentamidine	S100PRAGE	Other
Torcetrapib	cholesterol ester transfer protein	Other
Miltefosine	phospholipid antimicrobial drug	Other
Azaguanine-8	guanine analog	Other

Table 3.

Summary of inhibitory activity against monoacylglycerol lipase (MAGL).

Compound Name	Mechanism of Action	MAGL inhibitory activity (IC50)
CHEMBL130098	Hormone sensitive lipase	14 nM
CHEMBL1082517	Lysosomal acid lipase (LIPA)	3100 nM
JZL184	Monoacyl glycerol lipase(MAGL)	10 nM

General conclusion

Chemical screening has attracted attention in understanding novel biological phenomena by recent remarkable progress in science and technology. Successful chemical screening requires sophisticated primary phenotypic screening assay systems for identifying hit compounds and precise compound profiling for revealing the mechanisms of action and target proteins of the hit compounds. I tried to establish highly informative chemical screening platform to identify hit compounds and their target molecules, and furthermore to analyze how hit compounds induce the desired phenotype.

In the first chapter, in order to visualize the elementary processes of autophagy and identify factors involved in autophagy control, I have immunostained not only LC3 which is widely recognized as an autophagic marker, but also p62, rab7, and LAMP2. I established quantification methods of each protein, and by using these parameters, chemical screening for autophagy regulators was performed. In my study, 11 compounds that inhibited autophagy were identified and I focused on vacuolin-1 which was a target unknown compound. Target identification of vacuolin-1, one of the hit compounds, was performed by clustering analysis that developed and utilized an algorithm to quantify the morphology of cells based on image information of drug-treated cells. As a result, it was found that vacuolin-1 is an inhibitor of the lipid kinase PIKfyve which is involved in

the phosphorylation of phosphatidylinositol, and the transport of the lysosomal protein occurring during the transition from the Golgi apparatus to the lysosome is inhibited to induce autophagy. Other groups also reported that vacuolin-1 inhibited autophagy via suppressing lysosomal maturation [60], and these results strongly support my results. In this study, I obtained several types of autophagy inhibitors but, autophagy inducing compounds which could be novel drug candidates for several diseases, especially central nervous system related diseases were not found. It has recently been reported that BRD4 (Bromodomain-containing protein 4) inhibitors activate autophagy via direct lysosomal activation [99-102]. BRD4 is a member of the BET family, functions as a epigenetic modulator [103], and inhibition of BRD4 activity induces transcriptional activation of lysosomal genes. Since BRD4 inhibitor was not included in the library of our screening, a larger scale chemical screening by using my established screening platform makes it possible to obtain autophagy inducing compounds. In addition, some groups have recently developed improved methods for monitoring autophagy. Farkas et al. have developed luciferase-based detection system for autophagy flux [104], and Kaizuka et al. have debeloped GFP-LC3-RFP-LC3ΔG, a fluorescent probe to evaluate autophagic flux [105], Combining my method and other reported method will allow me to consider the mechanism of autophagy more deeply.

In the second chapter, SPT inhibitor was discovered as a target of a new anticancer drug that controls cancer metabolism, and its mechanism of action was elucidated. Little has been reported about the mechanism of action of SPT inhibitors, I have constructed a biologically annotated library and constructed a chemical screening system applied from the combination study of compounds. As a result of screening and following detailed analysis, SPT inhibitor promotes cell death by activating prostaglandin production pathway through induction of COX-2 expression. These data suggest that SPT inhibitor may be effective as anticancer agents in cancer types where COX-2 and prostaglandin pathway is activated. These findings are also interesting in that they can be used as patient stratification markers when conducting clinical trials using SPT inhibitors. In addition, my combination screening using annotation library with anti-cancer drug could be applied to MOA analysis of various anti-cancer drugs. In fact, I clarified the mechanism of action as an anticancer agent of another lipid synthase, SCD1 inhibitor by our established combination screening [106]. In summary, I conducted chemical screening and development of image-analysis algorithms, and clarified the control mechanism of autophagy and elucidated the MOA of anticancer drugs. My result is significant not only in contributing to the understanding of unknown biological phenomena but also in establishing methods for exploring and utilizing

compounds useful for medical care.

Acknowledgements

I am most grateful to Professor Tomiki Chiba, and Associate Professors Kentaro Nakano, Chikafumi Chiba, and Hidekazu Kuwayama, University of Tsukuba, for their continuous guidance and valuable discussions through my doctoral program.

I gratefully acknowledge Taro Nakazawa and Noriko Oshima, GE Healthcare Japan Corporation, for technical support of analyses using the IN Cell Analyser 6000 and IN Cell Developer Toolbox, Hiroyuki Sakuma for establishment of H4 cells expressing mCherry-GFP LC3, Takuto Kojima, Yasutomi Asano, Bunnai Saito, Tzu-Tshin Wong, Yasuhiro Hirata, Yuta Tanaka, Naoki Iwamura, Ryosuke Arai, Kazuko Yonemori, Yasufumi Miyamoto, Shuji Kitamura, and Shinichi Imamura for design and synthesis of SPT inhibitors, Masako Sasaki for measuring MAGL enzymatic activity, and Kaori Ito for technical assistance. I also deeply acknowledge Ikuo Miyahisa for critical discussions and editing, Junji Matsui and Naoki Tarui for providing encouragement for my study.

References

1. Ueno, T. & Nagano, T. (2011) Fluorescent probes for sensing and imaging, *Nat Meth.* **8**, 642-645.
2. Terai, T. & Nagano, T. (2008) Fluorescent probes for bioimaging applications, *Curr Opin Chem Biol.* **12**, 515-521.
3. Hanson, G. T. & Hanson, B. J. (2008) Fluorescent probes for cellular assays, *Comb Chem High Throughput Screen.* **11**, 505-513.
4. Frye, S. V. (2010) The art of the chemical probe, *Nat Chem Biol.* **6**, 159-161.
5. Kornienko, O., Lacson, R., Kunapuli, P., Schneeweis, J., Hoffman, I., Smith, T., Alberts, M., Inglese, J. & Strulovici, B. (2004) Miniaturization of whole live cell-based GPCR assays using microdispensing and detection systems, *J Biomol Screen.* **9**, 186-195.
6. Sundberg, S. A. (2000) High-throughput and ultra-high-throughput screening: solution- and cell-based approaches, *Current Opinion in Biotechnology.* **11**, 47-53.
7. Burbaum, J. J. (1998) Miniaturization technologies in HTS: how fast, how small, how soon?, *Drug Discovery Today.* **3**, 313-322.
8. Major, J. (1998) Challenges and Opportunities in High Throughput Screening: Implications for New Technologies, *Journal of Biomolecular Screening.* **3**, 13-17.
9. Moffat, J. G., Vincent, F., Lee, J. A., Eder, J. & Prunotto, M. (2017) Opportunities and challenges in phenotypic drug discovery: an industry perspective, *Nature reviews Drug discovery.* **16**, 531-543.
10. Wagner, Bridget K. & Schreiber, Stuart L. The Power of Sophisticated Phenotypic Screening and Modern Mechanism-of-Action Methods, *Cell Chemical Biology.* **23**, 3-9.
11. Haasen, D., Schopfer, U., Antczak, C., Guy, C., Fuchs, F. & Selzer, P. (2017) How Phenotypic Screening Influenced Drug Discovery: Lessons from Five Years of Practice, *Assay Drug Dev Technol.* **15**, 239-246.
12. Kosaka, T., Okuyama, R., Sun, W., Ogata, T., Harada, J., Araki, K., Izumi, M., Yoshida, T., Okuno, A., Fujiwara, T., Ohsumi, J. & Ichikawa, K. (2005) Identification of molecular target of AMP-activated protein kinase activator by affinity purification and mass spectrometry, *Anal Chem.* **77**, 2050-2055.
13. Gray, N. S. (2006) Drug discovery through industry-academic partnerships, *Nat Chem Biol.* **2**, 649-653.
14. Boutros, M., Heigwer, F. & Laufer, C. Microscopy-Based High-Content Screening, *Cell.* **163**, 1314-1325.

15. Thomas, N. (2010) High-content screening: a decade of evolution, *J Biomol Screen.* **15**, 1-9.
16. Ito, T., Ando, H., Suzuki, T., Ogura, T., Hotta, K., Imamura, Y., Yamaguchi, Y. & Handa, H. (2010) Identification of a primary target of thalidomide teratogenicity, *Science.* **327**, 1345-1350.
17. Sato, S., Murata, A., Shirakawa, T. & Uesugi, M. (2010) Biochemical target isolation for novices: affinity-based strategies, *Chem Biol.* **17**, 616-623.
18. Shi, H., Cheng, X., Sze, S. K. & Yao, S. Q. (2011) Proteome profiling reveals potential cellular targets of staurosporine using a clickable cell-permeable probe, *Chem Commun (Camb).* **47**, 11306-11308.
19. He, G., Luo, W., Li, P., Remmers, C., Netzer, W. J., Hendrick, J., Bettayeb, K., Flajolet, M., Gorelick, F., Wennogle, L. P. & Greengard, P. (2010) Gamma-secretase activating protein is a therapeutic target for Alzheimer's disease, *Nature.* **467**, 95-98.
20. Fukuda, Y., Sano, O., Kazetani, K., Yamamoto, K., Iwata, H. & Matsui, J. (2016) Tubulin is a molecular target of the Wnt-activating chemical probe, *BMC Biochemistry.* **17**, 9.
21. Michael, S., Auld, D., Klumpp, C., Jadhav, A., Zheng, W., Thorne, N., Austin, C. P., Inglese, J. & Simeonov, A. (2008) A robotic platform for quantitative high-throughput screening, *Assay Drug Dev Technol.* **6**, 637-657.
22. Bray, M. A., Singh, S., Han, H., Davis, C. T., Borgeson, B., Hartland, C., Kost-Alimova, M., Gustafsdottir, S. M., Gibson, C. C. & Carpenter, A. E. (2016) Cell Painting, a high-content image-based assay for morphological profiling using multiplexed fluorescent dyes, *Nat Protoc.* **11**, 1757-1774.
23. Lee, J. & Bogyo, M. (2013) Target deconvolution techniques in modern phenotypic profiling, *Curr Opin Chem Biol.* **17**, 118-126.
24. Schirle, M. & Jenkins, J. L. (2016) Identifying compound efficacy targets in phenotypic drug discovery, *Drug Discov Today.* **21**, 82-89.
25. Woo, J. H., Shimoni, Y., Yang, W. S., Subramaniam, P., Iyer, A., Nicoletti, P., Rodríguez Martínez, M., López, G., Mattioli, M., Realubit, R., Karan, C., Stockwell, B. R., Bansal, M. & Califano, A. Elucidating Compound Mechanism of Action by Network Perturbation Analysis, *Cell.* **162**, 441-451.
26. Sundaramurthy, V., Barsacchi, R., Chernykh, M., Stöter, M., Tomschke, N., Bickle, M., Kalaidzidis, Y. & Zerial, M. (2014) Deducing the mechanism of action of compounds identified in phenotypic screens by integrating their multiparametric profiles with a reference genetic screen, *Nat Protocols.* **9**, 474-490.

27. Sudbery, I., Enright, A. J., Fraser, A. G. & Dunham, I. (2010) Systematic analysis of off-target effects in an RNAi screen reveals microRNAs affecting sensitivity to TRAIL-induced apoptosis, *BMC Genomics.* **11**, 1-12.
28. Marine, S., Bahl, A., Ferrer, M. & Buehler, E. (2012) Common seed analysis to identify off-target effects in siRNA screens, *J Biomol Screen.* **17**, 370-378.
29. Mizushima, N., Levine, B., Cuervo, A. M. & Klionsky, D. J. (2008) Autophagy fights disease through cellular self-digestion, *Nature.* **451**, 1069-1075.
30. Wang, C., Machiraju, R. & Huang, K. (2014) Breast Cancer Patient Stratification using a Molecular Regularized Consensus Clustering Method, *Methods (San Diego, Calif).* **67**, 304-312.
31. Toss, A. & Cristofanilli, M. (2015) Molecular characterization and targeted therapeutic approaches in breast cancer, *Breast Cancer Research.* **17**, 60.
32. Swinney, D. C. & Anthony, J. (2011) How were new medicines discovered?, *Nature reviews Drug discovery.* **10**, 507-519.
33. Korn, K. & Krausz, E. (2007) Cell-based high-content screening of small-molecule libraries, *Current Opinion in Chemical Biology.* **11**, 503-510.
34. Young, D. W., Bender, A., Hoyt, J., McWhinnie, E., Chirn, G.-W., Tao, C. Y., Tallarico, J. A., Labow, M., Jenkins, J. L., Mitchison, T. J. & Feng, Y. (2008) Integrating high-content screening and ligand-target prediction to identify mechanism of action, *Nat Chem Biol.* **4**, 59-68.
35. Futamura, Y., Kawatani, M., Kazami, S., Tanaka, K., Muroi, M., Shimizu, T., Tomita, K., Watanabe, N. & Osada, H. (2012) Morphobase, an encyclopedic cell morphology database, and its use for drug target identification, *Chem Biol.* **19**, 1620-1630.
36. Su, Y., Ge, J., Zhu, B., Zheng, Y. G., Zhu, Q. & Yao, S. Q. (2013) Target identification of biologically active small molecules via in situ methods, *Curr Opin Chem Biol.* **17**, 768-775.
37. Rix, U. & Superti-Furga, G. (2009) Target profiling of small molecules by chemical proteomics, *Nat Chem Biol.* **5**, 616-624.
38. Perlman, Z. E., Slack, M. D., Feng, Y., Mitchison, T. J., Wu, L. F. & Altschuler, S. J. (2004) Multidimensional drug profiling by automated microscopy, *Science.* **306**, 1194-1198.
39. Gustafsdottir, S. M., Ljosa, V., Sokolnicki, K. L., Anthony Wilson, J., Walpita, D., Kemp, M. M., Petri Seiler, K., Carrel, H. A., Golub, T. R., Schreiber, S. L., Clemons, P. A., Carpenter, A. E. & Shamji, A. F. (2013) Multiplex cytological profiling assay to measure diverse cellular states, *PLoS One.* **8**, e80999.

40. Futamura, Y., Kawatani, M., Kazami, S., Tanaka, K., Muroi, M., Shimizu, T., Tomita, K., Watanabe, N. & Osada, H. (2012) Morphobase, an Encyclopedic Cell Morphology Database, and Its Use for Drug Target Identification, *Chemistry & Biology*. **19**, 1620-1630.
41. Carpenter, A. E., Jones, T. R., Lamprecht, M. R., Clarke, C., Kang, I. H., Friman, O., Guertin, D. A., Chang, J. H., Lindquist, R. A., Moffat, J., Golland, P. & Sabatini, D. M. (2006) CellProfiler: image analysis software for identifying and quantifying cell phenotypes, *Genome Biol.* **7**, R100.
42. Rubinsztein, D. C. (2006) The roles of intracellular protein-degradation pathways in neurodegeneration, *Nature.* **443**, 780-786.
43. Levine, B. & Kroemer, G. (2008) Autophagy in the Pathogenesis of Disease, *Cell.* **132**, 27-42.
44. Weidberg, H., Shvets, E. & Elazar, Z. (2011) Biogenesis and Cargo Selectivity of Autophagosomes, *Annual Review of Biochemistry.* **80**, 125-156.
45. Nakatogawa, H., Suzuki, K., Kamada, Y. & Ohsumi, Y. (2009) Dynamics and diversity in autophagy mechanisms: lessons from yeast, *Nat Rev Mol Cell Biol.* **10**, 458-467.
46. Nakatogawa, H., Ichimura, Y. & Ohsumi, Y. (2007) Atg8, a ubiquitin-like protein required for autophagosome formation, mediates membrane tethering and hemifusion, *Cell.* **130**, 165-178.
47. Kabeya, Y., Mizushima, N., Ueno, T., Yamamoto, A., Kirisako, T., Noda, T., Kominami, E., Ohsumi, Y. & Yoshimori, T. (2000) LC3, a mammalian homologue of yeast Apg8p, is localized in autophagosome membranes after processing, *EMBO.* **19**, 5720-5728.
48. Huotari, J. & Helenius, A. (2011) Endosome maturation, *The EMBO Journal.* **30**, 3481-3500.
49. Russell, M. R. G., Nickerson, D. P. & Odorizzi, G. (2006) Molecular mechanisms of late endosome morphology, identity and sorting, *Current Opinion in Cell Biology*. **18**, 422-428.
50. Hyttinen, J. M. T., Niittykoski, M., Salminen, A. & Kaarniranta, K. (2013) Maturation of autophagosomes and endosomes: A key role for Rab7, *Biochimica et Biophysica Acta (BBA) - Molecular Cell Research.* **1833**, 503-510.
51. Jäger, S., Bucci, C., Tanida, I., Ueno, T., Kominami, E., Saftig, P. & Eskelinen, E.-L. (2004) Role for Rab7 in maturation of late autophagic vacuoles, *Journal of Cell Science.* **117**, 4837-4848.

52. Bombrun, A., Gerber, P., Casi, G., Terradillos, O., Antonsson, B. & Halazy, S. (2003) 3,6-Dibromocarbazole Piperazine Derivatives of 2-Propanol as First Inhibitors of Cytochrome c Release via Bax Channel Modulation, *Journal of Medicinal Chemistry*. **46**, 4365-4368.
53. Fabian, M. A., Biggs, W. H., Treiber, D. K., Atteridge, C. E., Azimioara, M. D., Benedetti, M. G., Carter, T. A., Ciceri, P., Edeen, P. T., Floyd, M., Ford, J. M., Galvin, M., Gerlach, J. L., Grotzfeld, R. M., Herrgard, S., Insko, D. E., Insko, M. A., Lai, A. G., Lelias, J.-M., Mehta, S. A., Milanov, Z. V., Velasco, A. M., Wodicka, L. M., Patel, H. K., Zarrinkar, P. P. & Lockhart, D. J. (2005) A small molecule-kinase interaction map for clinical kinase inhibitors, *Nat Biotech.* **23**, 329-336.
54. Karaman, M. W., Herrgard, S., Treiber, D. K., Gallant, P., Atteridge, C. E., Campbell, B. T., Chan, K. W., Ciceri, P., Davis, M. I., Edeen, P. T., Faraoni, R., Floyd, M., Hunt, J. P., Lockhart, D. J., Milanov, Z. V., Morrison, M. J., Pallares, G., Patel, H. K., Pritchard, S., Wodicka, L. M. & Zarrinkar, P. P. (2008) A quantitative analysis of kinase inhibitor selectivity, *Nat Biotechnol.* **26**, 127-132.
55. Bjørkøy, G., Lamark, T., Brech, A., Outzen, H., Perander, M., Øvervatn, A., Stenmark, H. & Johansen, T. (2005) p62/SQSTM1 forms protein aggregates degraded by autophagy and has a protective effect on huntingtin-induced cell death, *The Journal of Cell Biology*. **171**, 603-614.
56. Pankiv, S., Clausen, T. H., Lamark, T., Brech, A., Bruun, J.-A., Outzen, H., Øvervatn, A., Bjørkøy, G. & Johansen, T. (2007) p62/SQSTM1 Binds Directly to Atg8/LC3 to Facilitate Degradation of Ubiquitinated Protein Aggregates by Autophagy, *Journal of Biological Chemistry*. **282**, 24131-24145.
57. Ohta, S., Inujima, Y., Abe, M., Uosaki, Y., Sato, S. & Miki, I. (2001) Inhibition of P-selectin specific cell adhesion by a low molecular weight, non-carbohydrate compound, KF38789, *Inflamm Res.* **50**, 544-551.
58. Reisen, F., Sauty de Chalon, A., Pfeifer, M., Zhang, X., Gabriel, D. & Selzer, P. (2015) Linking phenotypes and modes of action through high-content screen fingerprints, *Assay Drug Dev Technol.* **13**, 415-427.
59. Cerny, J., Feng, Y., Yu, A., Miyake, K., Borgonovo, B., Klumperman, J., Meldolesi, J., McNeil, P. L. & Kirchhausen, T. (2004) The small chemical vacuolin‐1 inhibits Ca2+‐dependent lysosomal exocytosis but not cell resealing, *EMBO reports.* **5**, 883-888.
60. Lu, Y., Dong, S., Hao, B., Li, C., Zhu, K., Guo, W., Wang, Q., Cheung, K.-H., Wong, C. W. M., Wu, W.-T., Markus, H. & Yue, J. (2014) Vacuolin-1 potently

and reversibly inhibits autophagosome-lysosome fusion by activating RAB5A, *Autophagy.* **10**, 1895-1905.

61. Jefferies, H. B. J., Cooke, F. T., Jat, P., Boucheron, C., Koizumi, T., Hayakawa, M., Kaizawa, H., Ohishi, T., Workman, P., Waterfield, M. D. & Parker, P. J. (2008) A selective PIKfyve inhibitor blocks PtdIns(3,5)P2 production and disrupts endomembrane transport and retroviral budding, *EMBO reports.* **9**, 164-170.
62. Martin, S., Harper, C. B., May, L. M., Coulson, E. J., Meunier, F. A. & Osborne, S. L. (2013) Inhibition of PIKfyve by YM-201636 dysregulates autophagy and leads to apoptosis-independent neuronal cell death, *PLoS One.* **8**, e60152.
63. Mizushima, N., Yoshimori, T. & Levine, B. Methods in Mammalian Autophagy Research, *Cell.* **140**, 313-326.
64. Kimura, S., Noda, T. & Yoshimori, T. (2007) Dissection of the autophagosome maturation process by a novel reporter protein, tandem fluorescent-tagged LC3, *Autophagy.* **3**, 452-460.
65. Martinez-Outschoorn, U. E., Peiris-Pages, M., Pestell, R. G., Sotgia, F. & Lisanti, M. P. (2017) Cancer metabolism: a therapeutic perspective, *Nature reviews Clinical oncology.* **14**, 11-31.
66. Yang, M., Soga, T. & Pollard, P. J. (2013) Oncometabolites: linking altered metabolism with cancer, *J Clin Invest.* **123**, 3652-3658.
67. Soga, T. (2013) Cancer metabolism: key players in metabolic reprogramming, *Cancer Sci.* **104**, 275-281.
68. Warburg, O., Wind, F. & Negelein, E. (1927) THE METABOLISM OF TUMORS IN THE BODY, *The Journal of General Physiology.* **8**, 519-530.
69. Pavlova, Natalya N. & Thompson, Craig B. (2016) The Emerging Hallmarks of Cancer Metabolism, *Cell Metabolism.* **23**, 27-47.
70. Hashimoto, A., Oikawa, T., Hashimoto, S., Sugino, H., Yoshikawa, A., Otsuka, Y., Handa, H., Onodera, Y., Nam, J.-M., Oneyama, C., Okada, M., Fukuda, M. & Sabe, H. (2016) P53- and mevalonate pathway–driven malignancies require Arf6 for metastasis and drug resistance, *The Journal of Cell Biology.* **213**, 81-95.
71. Olson, D. K., Fröhlich, F., Farese Jr, R. V. & Walther, T. C. (2016) Taming the sphinx: Mechanisms of cellular sphingolipid homeostasis, *Biochimica et Biophysica Acta (BBA) - Molecular and Cell Biology of Lipids.* **1861**, 784-792.
72. Hanada, K., Kumagai, K., Yasuda, S., Miura, Y., Kawano, M., Fukasawa, M. & Nishijima, M. (2003) Molecular machinery for non-vesicular trafficking of ceramide, *Nature.* **426**, 803-809.

73. Elojeimy, S., Liu, X., McKillop, J. C., El-Zawahry, A. M., Holman, D. H., Cheng, J. Y., Meacham, W. D., Mahdy, A. E., Saad, A. F., Turner, L. S., Cheng, J., T, A. D., Dong, J. Y., Bielawska, A., Hannun, Y. A. & Norris, J. S. (2007) Role of acid ceramidase in resistance to FasL: therapeutic approaches based on acid ceramidase inhibitors and FasL gene therapy, *Mol Ther.* **15**, 1259-1263.
74. Kawamori, T., Osta, W., Johnson, K. R., Pettus, B. J., Bielawski, J., Tanaka, T., Wargovich, M. J., Reddy, B. S., Hannun, Y. A., Obeid, L. M. & Zhou, D. (2006) Sphingosine kinase 1 is up-regulated in colon carcinogenesis, *Faseb j.* **20**, 386-388.
75. French, K. J., Schrecengost, R. S., Lee, B. D., Zhuang, Y., Smith, S. N., Eberly, J. L., Yun, J. K. & Smith, C. D. (2003) Discovery and evaluation of inhibitors of human sphingosine kinase, *Cancer Res.* **63**, 5962-5969.
76. Takai, A., Dang, H. T. & Wang, X. W. (2014) Identification of Drivers from Cancer Genome Diversity in Hepatocellular Carcinoma, *International Journal of Molecular Sciences.* **15**, 11142-11160.
77. Zhou, Q., Derti, A., Ruddy, D., Rakiec, D., Kao, I., Lira, M., Gibaja, V., Chan, H., Yang, Y., Min, J., Schlabach, M. R. & Stegmeier, F. (2015) A chemical genetics approach for the functional assessment of novel cancer genes, *Cancer Res.* **75**, 1949-1958.
78. Huang, S.-M. A., Mishina, Y. M., Liu, S., Cheung, A., Stegmeier, F., Michaud, G. A., Charlat, O., Wiellette, E., Zhang, Y., Wiessner, S., Hild, M., Shi, X., Wilson, C. J., Mickanin, C., Myer, V., Fazal, A., Tomlinson, R., Serluca, F., Shao, W., Cheng, H., Shultz, M., Rau, C., Schirle, M., Schlegl, J., Ghidelli, S., Fawell, S., Lu, C., Curtis, D., Kirschner, M. W., Lengauer, C., Finan, P. M., Tallarico, J. A., Bouwmeester, T., Porter, J. A., Bauer, A. & Cong, F. (2009) Tankyrase inhibition stabilizes axin and antagonizes Wnt signalling, *Nature.* **461**, 614-620.
79. Bornot, A., Blackett, C., Engkvist, O., Murray, C. & Bendtsen, C. (2014) The Role of Historical Bioactivity Data in the Deconvolution of Phenotypic Screens, *J Biomol Screen.* **19**, 696-706.
80. Liu, Y., Platchek, M., Kement, B., Bee, W. T., Truong, M., Zeng, X., Hung, S., Lin, H., Morrow, D., Kallal, L. A., Xie, Q., Agarwal, P., Pope, A. J. & Wu, Z. (2014) A novel approach applying a chemical biology strategy in phenotypic screening reveals pathway-selective regulators of histone 3 K27 tri-methylation, *Molecular BioSystems.* **10**, 251-257.
81. Polyakov, V. R., Moorcroft, N. D. & Drawid, A. (2014) Enrichment analysis for discovering biological associations in phenotypic screens, *J Chem Inf Model.* **54**, 377-386.

82. Wassermann, A. M., Camargo, L. M. & Auld, D. S. (2014) Composition and applications of focus libraries to phenotypic assays, *Front Pharmacol.* **5**, 164.
83. Fukuda, Y., Sano, O., Kazetani, K., Yamamoto, K., Iwata, H. & Matsui, J. (2016) Tubulin is a molecular target of the Wnt-activating chemical probe, *BMC Biochem.* **17**, 9.
84. Sano, O., Kazetani, K., Funata, M., Fukuda, Y., Matsui, J. & Iwata, H. (2016) Vacuolin-1 inhibits autophagy by impairing lysosomal maturation via PIKfyve inhibition, *FEBS Lett.* **590**, 1576-1585.
85. Yasutomi Asano, T. K., Osamu Kurasawa, Tzu-Tshin Wong, Yasuhiro Hirata, Naoki Iwamura, Bunnai Saito, Yuta Tanaka, Ryosuke Arai, Shinichi Imamura, Kazuko Yonemori, Yasufumi Miyamoto, Shuji Kitamura, and Osamu Sano (2016) Fused heterocyclic compound and application thereof. PCT/JP2016/062418 in
86. Bradford, M. M. (1976) A rapid and sensitive method for the quantitation of microgram quantities of protein utilizing the principle of protein-dye binding, *Analytical biochemistry.* **72**, 248-254.
87. Lee, Y. S., Choi, K. M., Choi, M. H., Ji, S. Y., Lee, S., Sin, D. M., Oh, K. W., Lee, Y. M., Hong, J. T., Yun, Y. P. & Yoo, H. S. (2011) Serine palmitoyltransferase inhibitor myriocin induces growth inhibition of B16F10 melanoma cells through G(2) /M phase arrest, *Cell Prolif.* **44**, 320-329.
88. Choi, K. E., Jung, Y. S., Kim, D. H., Song, J. K., Kim, J. Y., Jung, Y. Y., Eum, S. Y., Kim, J. H., Yoon, N. Y., Yoo, H. S., Han, S. B. & Hong, J. T. (2014) Myriocin induces apoptotic lung cancer cell death via activation of DR4 pathway, *Arch Pharm Res.* **37**, 501-511.
89. Shimada, K., Skouta, R., Kaplan, A., Yang, W. S., Hayano, M., Dixon, S. J., Brown, L. M., Valenzuela, C. A., Wolpaw, A. J. & Stockwell, B. R. (2016) Global survey of cell death mechanisms reveals metabolic regulation of ferroptosis, *Nat Chem Biol.* **12**, 497-503.
90. Conrad, M., Angeli, J. P. F., Vandenabeele, P. & Stockwell, B. R. (2016) Regulated necrosis: disease relevance and therapeutic opportunities, *Nature reviews Drug discovery.* **15**, 348-366.
91. Dixon, S. J., Lemberg, K. M., Lamprecht, M. R., Skouta, R., Zaitsev, E. M., Gleason, C. E., Patel, D. N., Bauer, A. J., Cantley, A. M., Yang, W. S., Morrison, B. & Stockwell, B. R. (2012) Ferroptosis: An Iron-Dependent Form of Non-Apoptotic Cell Death, *Cell.* **149**, 1060-1072.
92. Golstein, P. & Kroemer, G. Cell death by necrosis: towards a molecular definition, *Trends in Biochemical Sciences.* **32**, 37-43.

93. Dodo, K., Katoh, M., Shimizu, T., Takahashi, M. & Sodeoka, M. (2005) Inhibition of hydrogen peroxide-induced necrotic cell death with 3-amino-2-indolylmaleimide derivatives, *Bioorg Med Chem Lett.* **15**, 3114-3118.
94. de Bruin, E. C., Cowell, C., Warne, P. H., Jiang, M., Saunders, R. E., Melnick, M. A., Gettinger, S., Walther, Z., Wurtz, A., Heynen, G. J., Heideman, D. A. M., Gómez-Román, J., García-Castaño, A., Gong, Y., Ladanyi, M., Varmus, H., Bernards, R., Smit, E. F., Politi, K. & Downward, J. (2014) Reduced NF1 expression confers resistance to EGFR inhibition in lung cancer, *Cancer discovery.* **4**, 606-619.
95. Kerr, D. M., Harhen, B., Okine, B. N., Egan, L. J., Finn, D. P. & Roche, M. (2013) The monoacylglycerol lipase inhibitor JZL184 attenuates LPS-induced increases in cytokine expression in the rat frontal cortex and plasma: differential mechanisms of action, *Br J Pharmacol.* **169**, 808-819.
96. Dubois, R. N., Abramson, S. B., Crofford, L., Gupta, R. A., Simon, L. S., Van De Putte, L. B. & Lipsky, P. E. (1998) Cyclooxygenase in biology and disease, *Faseb j.* **12**, 1063-1073.
97. Ricciotti, E. & FitzGerald, G. A. (2011) Prostaglandins and Inflammation, *Arteriosclerosis, thrombosis, and vascular biology.* **31**, 986-1000.
98. Croxtall, J. D., van Hal, P. T. W., Choudhury, Q., Gilroy, D. W. & Flower, R. J. (2002) Different glucocorticoids vary in their genomic and non-genomic mechanism of action in A549 cells, *British Journal of Pharmacology.* **135**, 511-519.
99. Wen, X. & Klionsky, D. J. (2017) BRD4 is a newly characterized transcriptional regulator that represses autophagy and lysosomal function, 1-3.
100. Sakamaki, J. I. & Ryan, K. M. (2017) Transcriptional regulation of autophagy and lysosomal function by bromodomain protein BRD4, *Autophagy*, 0.
101. Sakamaki, J. I., Wilkinson, S., Hahn, M., Tasdemir, N., O'Prey, J., Clark, W., Hedley, A., Nixon, C., Long, J. S., New, M., Van Acker, T., Tooze, S. A., Lowe, S. W., Dikic, I. & Ryan, K. M. (2017) Bromodomain Protein BRD4 Is a Transcriptional Repressor of Autophagy and Lysosomal Function, *Autophagy.* **66**, 517-532.e9.
102. Sakamaki, J. I., Long, J. S., New, M., Van Acker, T., Tooze, S. A. & Ryan, K. M. (2017) Emerging roles of transcriptional programs in autophagy regulation, *Transcription*, 1-6.
103. Filippakopoulos, P. & Knapp, S. (2014) Targeting bromodomains: epigenetic readers of lysine acetylation, *Nature reviews Drug discovery.* **13**, 337-356.

104. Farkas, T., Hoyer-Hansen, M. & Jaattela, M. (2009) Identification of novel autophagy regulators by a luciferase-based assay for the kinetics of autophagic flux, *Autophagy*. **5**, 1018-1025.
105. Kaizuka, T., Morishita, H., Hama, Y., Tsukamoto, S., Matsui, T., Toyota, Y., Kodama, A., Ishihara, T., Mizushima, T. & Mizushima, N. (2016) An Autophagic Flux Probe that Releases an Internal Control, *Molecular cell*. **64**, 835-849.
106. Ono, A., Sano, O., Kazetani, K. I., Muraki, T., Imamura, K., Sumi, H., Matsui, J. & Iwata, H. (2017) Feedback activation of AMPK-mediated autophagy acceleration is a key resistance mechanism against SCD1 inhibitor-induced cell growth inhibition. **12**, e0181243.